forests

MDPI

Article

Assessment of Burned Area Products During the Severe Fire Season in the Xingu River Basin, Brazilian Amazon

Juarez Antonio da Silva Junior [1], Admilson da Penha Pacheco [2], Antonio Miguel Ruiz-Armenteros [3,4,5,*], José Anderson Estefano Silva de Souza [2] and Leidjane Maria Maciel de Oliveira [1]

[1] Department of Civil and Environmental Engineering, Federal University of Pernambuco, Av. Prof. Moraes Rego, 1235, Cidade Universitária, Recife 50670-901, Brazil; juarez.silvajunior@ufpe.br (J.A.d.S.J.); leidjane.oliveira@ufpe.br (L.M.M.d.O.)
[2] Department of Cartographic and Surveying Engineering, Center for Technology and Geosciences, Federal University of Pernambuco, Av. Prof. Moraes Rego, 1235, Cidade Universitária, Recife 50670-901, Brazil; admilson.pacheco@ufpe.br (A.d.P.P.); jose.aesilva@ufpe.br (J.A.E.S.d.S.)
[3] Department of Cartographic, Geodetic and Photogrammetry Engineering, University of Jaén, Campus Las Lagunillas s/n, 23071 Jaén, Spain
[4] Microgeodesia Jaén Research Group (PAIDI RNM-282), University of Jaén, Campus Las Lagunillas s/n, 23071 Jaén, Spain
[5] Center for Advanced Studies on Earth Sciences, Energy and Environment CEACTEMA, University of Jaén, Campus Las Lagunillas s/n, 23071 Jaén, Spain
* Correspondence: amruiz@ujaen.es

Abstract

This study evaluated the performance of four burned area products (AQ1Km, FireCCIS311, MCD64A1, and VNP64A1) using the reference datasets MapBiomas Fire and the Global Annual Burned Area Map (GABAM) for 2024. The two 30 m reference datasets are generated using different automated classification approaches, including deep learning in MapBiomas Fire and Random Forest in GABAM, allowing the sensitivity of product evaluation to alternative machine-learning-based reference frameworks to be examined. The Xingu River basin is a heterogeneous tropical landscape characterized by extensive forest ecosystems, protected and Indigenous territories, agricultural frontiers, and recurrent fire activity. Accuracy metrics derived from confusion matrices (contingency table metrics) were combined with analyses of burned scar geometry, burned patch size, land use and land cover, low-resolution grid regression, and Kernel Density Estimation (KDE) based on active fire hotspots. Results showed substantial differences among products in their ability to represent burned scars under tropical conditions. FireCCIS311 achieved the best overall performance, presenting the highest Intersection over Union (IoU) values (52.67% against MapBiomas Fire), better geometric coherence, and stronger spatial regression consistency (r^2 = 0.88). AQ1Km showed higher sensitivity and a stronger association with active fire hotspots, but also greater commission errors (CE) and spatial overestimation. MCD64A1 and VNP64A1 presented intermediate performance, with higher omission rates, particularly in forested and fragmented areas. All products showed low accuracy for small, burned patches, while performance improved for larger and more continuous scars. The results also highlighted the strong influence of the reference dataset on validation outcomes, with markedly better agreement observed with MapBiomas Fire than with GABAM. These results show that product uncertainty can alter the spatial evidence used to characterize wildfire impacts. Regionally validated and complementary burned area products can therefore provide a more reliable basis for forest fire monitoring, post-fire assessment, and operational fire management in heterogeneous tropical landscapes.

Check for updates

Academic Editor: Eman H. Alkhammash

Received: 10 September 2026
Revised: 2 October 2026
Accepted: 8 October 2026
Published: 16 October 2026

Copyright: © 2026 by the authors. Licensee MDPI, Basel, Switzerland. This article is an open access article distributed under the terms and conditions of the Creative Commons Attribution (CC BY) license.

Keywords: burned area mapping; forest fire monitoring; remote sensing; product validation; machine learning; MapBiomas Fire; GABAM; Brazilian Amazon

1. Introduction

The Amazon region, recognized for its immense biodiversity and for harboring unique ecosystems, has experienced a marked increase in wildfire activity, a trend increasingly associated with drought intensification, land use pressure, and changes in fire regimes under a changing climate. This problem becomes even more serious in its river basins, which play a fundamental role in supporting species, ecosystems, and native communities [1]. In addition to constituting the largest freshwater network on the planet, the Amazon acts as an important climate regulator, linking forest dynamics with regional conditions across several South American countries. Within this context, the Xingu River basin in Pará stands out as a strategic area for Amazonian conservation because it functions as a barrier against the advance of deforestation. However, the increase in wildfires directly threatens this function. This is particularly relevant because recurrent fires can weaken forest resilience, alter vegetation structure, and increase the vulnerability of protected and Indigenous territories to subsequent disturbances. In September 2024, more than 60,000 hectares were consumed by fire in the region, reaching areas that are difficult to access and Indigenous Lands within the basin [2]. Furthermore, in areas near Indigenous lands, agricultural expansion and deforestation practices continue to be associated with the use of fire as a land-clearing tool. Local communities have reported changes in wildlife distribution, including game species and fish, potentially associated with fire-related environmental stressors and increased river-water temperatures. In addition, smoke from the wildfires can worsen health problems because it contains fine particulate matter (PM2.5), which can cause serious impacts on human health both locally and across broader regions [3,4]. Together, these environmental and land use pressures make the Xingu basin a particularly complex region for forest fire monitoring, where fire occurrence interacts with forest conservation, landscape transformation, and human activities.

With the intensification of land use practices associated with fire and the increased occurrence of fires caused by human activity, remote sensing applications have become fundamental to understanding the historical and current dynamics of these events, especially in large, remote, and difficult-to-access tropical forest regions. Remote sensing allows for the assessment of fire impacts at different spatial scales and contributes to near-real-time monitoring [5,6]. From a remote sensing perspective, the effects caused by forest fires can be interpreted as abrupt and temporary changes in the spectral response of vegetation cover. According to Chuvieco et al. [7], there are two main types of remote sensing products applied to fire studies: those related to heat, which identify active fires, thermal anomalies, or hotspots, and those focused on the biophysical changes observed in vegetation after fire occurrence, which are commonly used to map burned areas. In recent years, hybrid strategies that combine changes in post-fire reflectance with the thermal contrast from active fires or hotspots have been widely used. These approaches integrate the advantages of each method, providing operationally efficient alternatives with improved capacity for detecting and analyzing fire events [8,9]. Beyond their scientific use, burned area products contribute to the evidence used to identify recurrent fire zones, assess impacts across land cover types, and prioritize monitoring and management actions. In heterogeneous territories, systematic omission (OE) and commission errors (CE) may therefore affect not only estimates of burned extent, but also the spatial information available for wildfire surveillance, post-fire assessment, and operational fire management.

Several regional and global algorithms for detecting and assessing burned areas have been developed over the years, mainly using data from moderate- to coarse-spatial-resolution sensors [10]. Among the most widely used products are those derived from the MODIS sensor, such as NASA's MCD64A1, which provides burned area information at 500 m spatial resolution and has been continuously available since 2000 [11,12]. Furthermore, Collection 2 of the VIIRS Global Burned Area Product (VNP64A1) was created to ensure the continuity of the historical record of burned areas obtained by MODIS [13]. Another important set of products is Fire_CCI, developed within the framework of the ESA Climate Change Initiative, with spatial resolutions that vary among products. This set includes FireCCI50, available between 2001 and 2016 [14], and FireCCI51, with data from 2001 to 2020 [15]. More recently, new burned area products have begun to use data from the OLCI sensor aboard Sentinel-3. Among them, the C3SBA10 stands out, developed by the Copernicus Climate Change Service (C3S) of the European Commission, and available since 2016 [16]. The CLMBA40nrt and CLMBA40ntc sets were also developed, based on data from the OLCI and SLSTR sensors onboard the Sentinel-3A and Sentinel-3B satellites [17], in addition to FireCCIS310, derived from SYNERGY data from Sentinel-3 [18]. Before this, MERIS sensors with a spatial resolution of 300 m had already been used for mapping burned areas between 2005 and 2011 [8,19]. On a regional scale, the AQ1Km product, developed by the Brazilian Laboratory of Environmental Satellite Applications in partnership with the National Institute for Space Research (INPE), stands out. This product provides information on burned areas throughout South America, covering the period from 2001 to the present day [20,21]. Despite this broad availability of global and regional burned area datasets, their performance can vary substantially across tropical forest environments because of differences in sensor resolution, detection algorithms, temporal compositing, and the incorporation of active fire information.

All the burned area products mentioned have already been extensively validated in different fire-prone biomes, including boreal forests, the Amazon, swamps, Mediterranean scrublands, pine forests, the Cerrado, tropical forests, wooded savannas, and grasslands. However, due to the high complexity and rapid dynamics of fire-induced changes in the Amazon biome, further studies are still needed to evaluate the performance of these products in this region, particularly under conditions of increasing drought stress, land use change, and recurrent fire activity [22–27]. According to Chuvieco et al. [7], the difficulties in automating burned area detection using satellite imagery are mainly related to the complexity of the variables involved, the algorithms used, the spectral heterogeneity of the landscape, and atmospheric conditions. In this context, factors such as fire regimes, climatic and environmental conditions, as well as the characteristics of different optical sensors, directly influence the quality of the products generated. Similarly, Giglio et al. [13], in a validation study of the VNP64A1 product in the tropical savanna of northern South America, highlighted limitations associated with spatial resolution, high cloud cover, and vegetation type, factors that hinder the precise mapping of burned areas. Stroppiana et al. [24], when comparing the FireCCISFD20, FireCCI51, FireCCIS311, and MCD64A1 products in African biomes, as well as Valencia et al. [28], in a global analysis involving the MCD45, MCD64C5.1, MCD64C6, FireCCI C4.1, and FireCCI C5.0 products, also identified limitations related to environmental variables, such as the presence of aerosols, vegetation type, landscape fragmentation, spatial and temporal resolution of the sensors, and the time of orbital passage. These factors directly influence the extent of burned areas detected by the global products and, consequently, the accuracy of the data obtained [10]. Furthermore, the authors highlight that different fire regimes, climatic conditions, land cover, spectral bands used, sensor observation frequency, and shading effects also contribute to the occurrence of spectral confusion, further hindering the accurate detection of burned scars [6,8,29].

These limitations are evidenced by the high variability in accuracy metrics reported for different burned area products. Several studies have evaluated the performance of these products using independent high-spatial-resolution reference data, generally derived from Landsat and Sentinel imagery at approximately 10–30 m spatial resolution, interpreted visually or compared pairwise [30]. Hall et al. [31], for example, when analyzing forest fires in Ukraine, reported high OE for the MCD64A1 (71%–76%) and FireCCI51 (63%–99%) products, as well as high CE for the MCD64A1 (62%–81%) and FireCCI51 (49%–93%). Similarly, Stage 3 validation of the MCD64A1 product showed a CE of 40.2% and an OE of 72.6%, in addition to a relative bias of –54% [12]. For FireCCI, Padilla et al. [32] reported a CE of 54% and an OE of 67%, with an approximate underestimation of 28%. In another environmental context, Huang et al. [33], in the Tibetan Plateau, observed better performance of FireCCI51 compared to MCD64A1, registering lower values of CE (MCD64A1: 68.09%; FireCCI51: 31.37%) and OE (MCD64A1: 58.41%; FireCCI51: 47.56%). Khairoun et al. [34], in a recent validation exercise, obtained Dice coefficients of 0.71 for MCD64A1 and 0.73 for FireCCI51, indicating relatively similar performance between the products. These results illustrate how global burned area products are subject to different levels of inaccuracy, influenced by environmental characteristics, the sensors used, and the detection algorithms themselves. Consequently, the continuous improvement of these products and the development of new validation studies become fundamental. Thus, given the high variability in results and the differences in sensitivity and applicability among the products, the systematic evaluation of their accuracy has become an indispensable step, especially in regions where fire monitoring supports forest conservation, risk management, and climate adaptation strategies [35,36].

The increasing use of automated and machine-learning-based approaches for burned area mapping also makes the selection of reference data particularly important. In the present study, MapBiomas Fire and GABAM represent two distinct automated mapping frameworks: MapBiomas Fire uses a Deep Neural Network approach regionally calibrated for Brazilian biomes, whereas GABAM is based on a Random Forest classification framework with global coverage [27]. Comparing the evaluated burned area products independently against these two references therefore provides an opportunity to examine how the choice of automated reference mapping framework influences product assessment.

Given this context, the present study evaluates the performance of four global and regional burned area products—AQ1Km, FireCCIS311, MCD64A1, and VNP64A1—in the Xingu River basin, Brazilian Amazon, using MapBiomas Fire and GABAM as separate higher-spatial-resolution reference datasets. The analysis combines pixel-based accuracy metrics (OA, CE, OE, and IoU) with complementary assessments of burned scar geometry, patch size, land use and land cover, low-resolution grid regression, and the spatial distribution of active fire hotspots. By applying this multidimensional framework to a heterogeneous and fire-prone Amazonian basin, the study examines both differences among burned area products and the sensitivity of validation outcomes to the choice of reference dataset. This approach provides a regionally focused assessment of product performance and mapping uncertainty, with implications for the selection and interpretation of burned area datasets used in wildfire monitoring, post-fire assessment, and environmental management.

To our knowledge, this study provides the first comprehensive assessment of four major global and regional burned area products specifically focused on the Xingu River basin, a critical deforestation and fire-prone frontier in the Brazilian Amazon. Its main contribution lies in evaluating not only product performance, but also the sensitivity of validation outcomes to the choice of reference dataset by separately comparing MapBiomas Fire and GABAM. In addition, the study goes beyond traditional confusion matrix metrics

by integrating burned scar geometry, burned patch size analysis, land use and land cover stratification, low-resolution grid regression, and kernel density analysis based on active fire hotspots. This multidimensional framework allows a more detailed assessment of how landscape fragmentation, land cover heterogeneity, and burned area extent influence OE and CE in complex Amazonian environments. The Xingu basin is therefore examined not only as a technically challenging tropical forest environment in which reliable burned area information is particularly relevant to wildfire monitoring, conservation assessment, and integrated fire management.

2. Materials and Data

2.1. Study Area

The study area encompasses the Xingu River basin, which extends for approximately 2500 km across the states of Mato Grosso and Pará and consists of a mosaic of ecosystems that include dense forests, Amazonian floodplains, and Cerrado areas (Figure 1). Within its territory lies the Xingu Protected Areas Corridor, one of the largest continuous forest mosaics composed of Indigenous Lands (ILs) and Conservation Units (CUs) on the planet. This basin has a dense hydrographic network and is of great importance to Amazonian biodiversity and Indigenous cultures, in addition to contributing about 4% of the annual discharge of the Amazon River [3,37]. The basin boundary used in this study was obtained from the Metadata Catalog of the National Water and Basic Sanitation Agency (ANA) (https://metadados.snirh.gov.br, accessed on 9 May 2026) [38], and the area analyzed covers approximately 531,250 km^2.

This region was selected due to its high ecological, environmental, and hydrological relevance at regional and global scales, as well as being located within the Arc of Deforestation, an area that concentrates the highest rates of deforestation and wildfires in the country. The Xingu basin is protected by a broad mosaic of protected areas, composed of Indigenous Lands and state and federal Conservation Units, which are fundamental for containing deforestation and maintaining the hydrological cycle [39]. However, these areas are frequently affected by fires, which can cause biodiversity loss and increase health risks for traditional peoples because of smoke exposure. In this context, the region faces increasingly intense drought events, with studies pointing to significant reductions in river flow and increased duration of drought periods. These hydroclimatic changes can increase fuel dryness and fire susceptibility, making the basin an especially relevant area for evaluating burned area monitoring products under changing environmental conditions [40,41]. Drought dynamics and water stress in the Amazon rainforest differ markedly from regions such as Mediterranean landscapes. While Mediterranean ecosystems feature vegetation adapted to and highly flammable during seasonal drought, fuel moisture in the Amazon is regulated by a dense, humid tropical structure. Consequently, the resulting fire behavior is incomparable, often manifesting as low-intensity surface fires beneath the closed canopy. This understory burning masks the spectral signal and hinders detection by remote sensors, leading to high omission rates that do not occur in biomes with more open vegetation [42]. In addition to representing an important territory for Indigenous peoples and environmental conservation, the basin is also marked by conflicts related to land use. This situation is further intensified by the strong pressure exerted by agricultural expansion and illegal logging, which can contribute to the high incidence of forest fires [1–3]. The Xingu basin therefore represents a complex forest landscape in which conservation areas, Indigenous Lands, agricultural expansion, forest change, and recurrent fire activity coexist. These characteristics make the basin particularly suitable for evaluating the reliability of burned area products under heterogeneous tropical forest conditions and for assessing their potential use in wildfire monitoring and management.

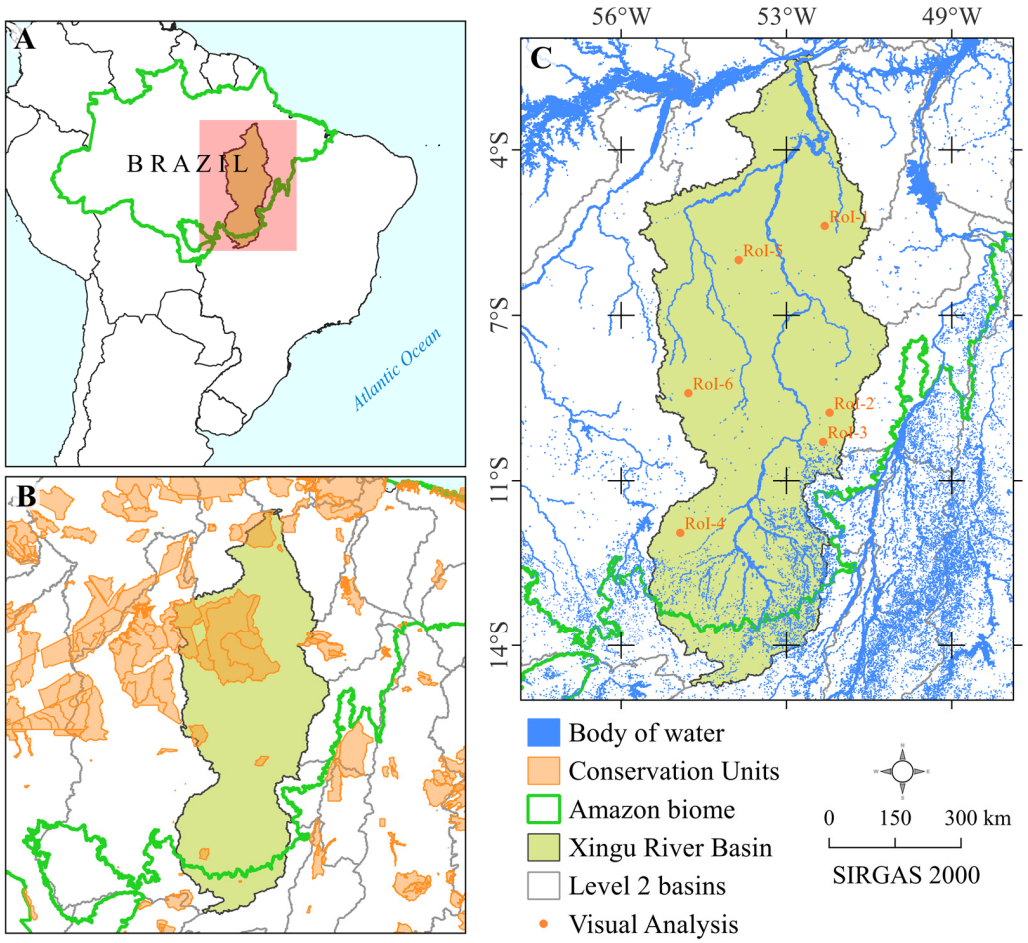


Figure 1. Geographic location and spatial characterization of the Xingu River basin, Brazilian Amazon. (**A**) Location of the Xingu River basin within Brazil; (**B**) spatial distribution of conservation units and the basin boundary in relation to the Amazon biome; and (**C**) hydrographic network, basin boundaries, and spatial distribution of the six regions of interest (ROIs) selected for the visual comparison of burned area products and reference datasets. Coordinate reference system: SIRGAS 2000.

2.2. Burned Area Products

Table 1 presents the main characteristics of the burned area products used in this study, including spatial coverage, spatial and temporal resolution, availability period, primary input data, and respective bibliographic references. Four products widely used in fire monitoring were evaluated: AQ1Km, FireCCIS311, MCD64A1, and VNP64A1. All products have a monthly temporal frequency and differ in terms of temporal coverage and the sensors used in detecting burned areas.

Collection 2 of the AQ1Km Burned Area product results from a complete reprocessing of the previous version, based on new data evaluation and validation, aiming for greater reliability, spatial consistency, and completeness through the integration of active fire detections from MODIS sensors, allowing the inclusion of pixels associated with active fires surrounding burned areas. Updated masks for potential false-detection sources, such as industries and solar farms, were also applied, reducing false positives and increasing the robustness of the product [20]. The Sentinel-3 S3 SYN (Synergy) Fire_cci version 1.1 product, here referred to as FireCCIS311, consists of global monthly burned area maps with a spatial resolution of 300 m, covering the period from 2019 to 2024. It is generated from the Synergy dataset, developed using the OLCI (Ocean and Land Colour Instrument) and SLSTR (Sea and Land Surface Temperature Radiometer) sensors onboard Sentinel-3 satellites. The algorithm uses Synergy level 2 surface reflectance and active fire data from

VIIRS as its main inputs. The product focuses on mapping burned areas, also incorporating observations of active fires as complementary information, in order to improve the detection of burned areas in different types of biomes [18].

Table 1. Main characteristics of the burned area products used in this study: AQ1Km, FireCCIS311, MCD64A1, and VNP64A1. FireCCIS311 corresponds to the Sentinel-3 Synergy Fire_cci product version 1.1.

Product	Spatial Coverage	Spatial Resolution (m)	Temporal Frequency	Temporal Coverage	Primary Input Data	References	Burned Area in the Basin in 2024 (km^2)
AQ1Km	South America	1000	Monthly	2001–present	MODIS Sentinel-3	[20]	44,400
FireCCIS311	Global	300	Monthly	2019–2024	SYN, VIIRS active fires	[18]	32,200
MCD64A1	Global	500	Monthly	2000–present	MODIS	[13]	29,000
VNP64A1	Global	500	Monthly	2014–present	VIIRS	[41]	30,000
Mapbiomas Fire	South America	30	Monthly	1985–2025	Landsat/ Sentinel-2	[43]	40,800
GABAM	Global	30	Annual	1986–2025	Landsat	[44]	12,500

The MCD64A1 Burned Area from the MODIS Collection 6.1, developed by NASA, provides global monthly maps of burned areas with a spatial resolution of 500 m, covering the period from November 2000 to the present. This product is generated from the combination of MODIS surface reflectance data with thermal anomaly information derived from MODIS active fire observations. The algorithm employs a burn-sensitive vegetation index to define dynamic thresholds applied to composite data, using atmospherically corrected surface reflectance and incorporating a temporal texture metric [11]. The VNP64A1 product, version 1, derived from the VIIRS (Visible Infrared Imaging Radiometer Suite) sensor aboard NASA's Suomi NPP satellite, consists of a monthly global gridded dataset with a spatial resolution of 500 m, containing per-pixel information on burned areas and quality indicators. The methodology employed uses VIIRS imagery combined with observations of active fires from the sensor itself. For burned area detection, VIIRS spectral bands sensitive and insensitive to biomass burning are used, allowing the identification of fire-induced changes and their differentiation from other types of surface changes [13,42]. For all products, the analysis was conducted for 2024, ensuring temporal consistency with the reference burned area datasets used in the validation. Monthly layers were aggregated or compared according to the temporal resolution of each reference dataset, as described in Section 3.

2.3. Reference Datasets

As described in the International Global Burned Area Satellite Product Validation Protocol [45], the use of validation data with higher spatial resolution is fundamental in the evaluation of burned area maps, as it allows for a more precise representation of the boundaries and heterogeneity of burned scars, making it possible to detect small, fragmented fires with complex geometry, which are often not captured by sensors with coarser spatial resolution [7,28]. In this context, in order to reduce dependence on a single reference dataset and to evaluate the consistency of the performance of coarse-resolution burned area products against different higher-resolution sources, this study used two reference products separately: MapBiomas Fire and the Global Annual Burned Area Map (GABAM), both with a spatial resolution of 30 m. Although both reference datasets have a finer spatial resolution than the evaluated products, they are also subject to

uncertainties related to cloud cover, acquisition frequency, classification algorithms, and temporal compositing. Therefore, they were used as separate reference datasets rather than as error-free ground truth. Using both reference datasets also makes it possible to examine whether alternative sources of geospatial evidence lead to different interpretations of wildfire extent and product reliability across the basin's land use contexts.

Collection 4 of MapBiomas Fire presents annual and monthly mapping of burned scars in Brazil from 1985 to 2024, based on Landsat mosaics and auxiliary data on active fire hotspots from INPE (National Institute for Space Research), and is widely used as a reference dataset for validation due to its high spatial resolution and temporal consistency. MapBiomas Fire was developed collaboratively by institutions belonging to the MapBiomas network, using a Deep Neural Network (DNN) model, implemented on the Google Earth Engine and Google Cloud Platform, which offer high-performance cloud-processing capacity, complemented by local infrastructure [27,30]. The MapBiomas Fire data, georeferenced in the WGS84 system and provided in GeoTIFF format, can be freely downloaded at https://brasil.mapbiomas.org/ (accessed on 2 April 2026) [43]. In this study, MapBiomas Fire was used as a regional reference dataset because it is specifically developed for Brazilian biomes and provides burned area information at a spatial resolution compatible with Landsat-based validation.

Using an automated approach for global burned area mapping from Landsat 7 and 8 satellite imagery, Long et al. [46] developed the original GABAM product for global burned area mapping. An updated 30 m GABAM dataset covering 2014–2024 is available through Zenodo (https://zenodo.org/records/13858799, accessed on 2 April 2026) [44], and the 2024 layer was used in this study. GABAM was produced through an automated pipeline implemented on the Google Earth Engine platform, using machine learning algorithms based on Random Forest classification combined with spectral indices. The data are available in geographic coordinates (latitude/longitude), using the WGS84 horizontal datum, organized in 10° × 10° mosaics, covering the spatial extent between 180° W–180° E and 80° N–60° S [47,48]. Additional information on the GABAM algorithm and processing can be found in Long et al. [46]. The two reference datasets were analyzed separately to avoid merging products with different algorithmic assumptions, temporal structures, and regional calibrations. This approach allowed the sensitivity of product performance to the choice of reference dataset to be explicitly assessed.

3. Methods

Figure 2 summarizes the overall analytical workflow adopted in this study. The workflow was organized into five interconnected components: (i) input datasets, including the burned area products, reference datasets, and auxiliary data; (ii) data preprocessing and spatial harmonization within the Xingu River basin; (iii) pixel-based accuracy assessment and complementary analyses of burned scar geometry, patch size, land use and land cover context, aggregated grid agreement, and active fire hotspot density; (iv) integration and interpretation of the results; and (v) comparative outputs and implications for forest fire monitoring and management. This multidimensional framework was designed to evaluate product performance from complementary perspectives, including classification accuracy, spatial agreement, geometric representation, and landscape context. The detailed procedures applied in each analytical component are described below.

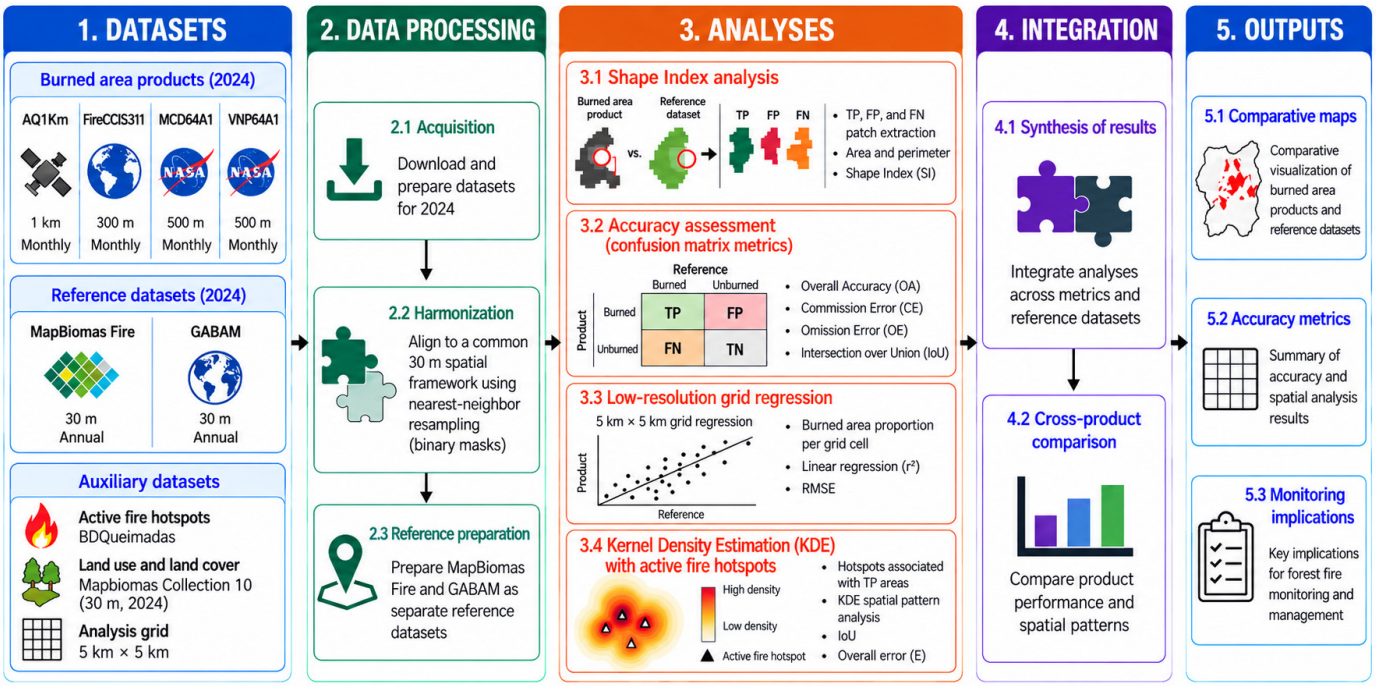


Figure 2. Overall analytical workflow adopted to evaluate and interpret the performance of burned area products in the Xingu River basin. The workflow is organized into five color-coded components: datasets (blue), data processing (green), analyses (orange), integration (purple), and outputs (blue). Arrows indicate the sequence of methodological steps and the connections between components, while graphical symbols illustrate the datasets, processing operations, analytical methods, and resulting outputs.

Before the accuracy assessment, all burned area products and reference datasets were clipped to the Xingu River basin boundary and harmonized to a common spatial framework. Because the evaluated products have different native spatial resolutions, the comparisons were performed using binary burned/unburned masks generated for each product and the reference datasets. Monthly burned area layers were aggregated according to the temporal window analyzed in this study, ensuring consistency between the evaluated products and the reference maps. All spatial overlays were conducted using the same coordinate reference system and basin mask to avoid differences caused by projection, extent, or grid alignment. Patch correspondence was determined based on spatial overlap rather than by imposing a one-to-one matching between reference and product patches. When a single reference patch overlapped multiple patches from an evaluated product, all spatially intersecting product patches were retained in the comparison rather than selecting only the largest or nearest patch. Thus, one-to-many patch correspondences were allowed, preserving the spatial configuration represented by each burned area product.

For the pixel-based accuracy assessment, all raster datasets were spatially aligned using the Align Rasters tool in QGIS. The burned area products at their native spatial resolutions of 1000 m (AQ1Km), 500 m (MCD64A1 and VNP64A1), and 300 m (FireCCIS311) were resampled to the 30 m spatial framework of the reference datasets using the Nearest Neighbor method. This method was selected because the burned/unburned maps were treated as categorical binary data, thereby preserving class values during resampling. The resampling procedure was used exclusively to enable grid alignment and pixel-by-pixel comparison and does not imply an increase in the effective spatial resolution of the original burned area products. Thus, a native coarse-resolution pixel is represented by multiple 30 m pixels carrying the same original class information, rather than by additional spatial information. Consequently, pixel-based accuracy metrics may remain affected by the native

spatial resolution, mixed-pixel effects, and spatial uncertainty along burned scar boundaries. For this reason, the pixel-based assessment was complemented by the 5 × 5 km aggregated grid analysis described in Section 3.3.

3.1. Shape Index Analysis

The Shape Index was used to characterize the geometric complexity and spatial regularity of the burned area patches identified by the evaluated products, allowing assessment of whether the products adequately reproduce the spatial complexity of burned scars, as well as identification of geometric patterns associated with OE and CE under different forms and levels of fragmentation [49,50]. In the present study, the Shape Index was calculated for the spatial groupings of pixels classified as true positives (TP), false positives (FP), and false negatives (FN), derived from the pixel-by-pixel comparison between each burned area product and the MapBiomas Fire and GABAM reference datasets.

Initially, binary masks corresponding to each evaluation class (TP, FP, and FN) were generated from the spatial comparison matrices. In this classification, TP represented pixels mapped as burned by both the evaluated product and the reference dataset, FP represented pixels mapped as burned only by the evaluated product, and FN represented pixels mapped as burned only by the reference dataset. Then, adjacent pixels were grouped into continuous patches using eight-neighbor connectivity, allowing the identification of spatially independent patches. For each patch, geometric properties, including area and perimeter, were extracted and used to calculate the Shape Index, which was subsequently summarized by product, reference dataset, and error class. The Shape Index (S) was calculated according to Equation (1):

$$S = \frac{P}{2\sqrt{\pi A}} \quad (1)$$

where P represents the perimeter of the patch, and A represents its area. The normalized shape metric ranges from 0 to 1, with values closer to 1 indicating more compact and geometrically regular spatial configurations, whereas lower values indicate progressively less compact, more irregular, or fragmented configurations.

3.2. Accuracy Analysis

For each product, confusion matrices were generated from pixel-by-pixel comparisons between the evaluated products and the MapBiomas Fire and GABAM reference datasets. From these matrices, the following metrics were derived: (i) OA, representing the total proportion of correct classifications; (ii) CE, expressing the proportion of pixels incorrectly classified as burned by the product; and (iii) OE, corresponding to reference burned pixels not detected by the product [51]. Because unburned pixels commonly dominate burned area validation datasets, OA was interpreted together with CE, OE, and IoU to avoid overestimating product performance. In addition to these metrics, the IoU was also obtained, which quantifies the degree of overlap between the evaluated product and the reference data [6]. The IoU value ranges from 0 to 1, where 1 indicates perfect overlap. The formula for IoU based on the components of the contingency table is (Equation (2)):

$$IoU = \frac{TP}{TP + FP + FN} \quad (2)$$

where TP represents true positive pixels, FP represents false positive pixels, and FN represents pixels classified as unburned by the product but burned in the reference dataset. Additionally, an analysis of product performance as a function of burned area size (patch size) was carried out based on IoU. The burned area polygons were grouped into seven

size classes (in km^2): 0–5 km^2, 5–10 km^2, 10–25 km^2, 25–50 km^2, 50–75 km^2, 75–100 km^2, and >100 km^2 [52].

Additionally, the IoU metric was used to assess the performance of the burned area products across different land use and land cover (LULC) classes within the Xingu River basin. As auxiliary data, the MapBiomas Collection 10 LULC product for 2024 was used as a georeferenced raster dataset with a spatial resolution of 30 m. The analysis focused on the predominant LULC classes within the study area: Forest Formation, Savanna Formation, Forestry, Flooded Forest and Pasture. The burned area products and reference datasets were spatially intersected with these LULC classes, and IoU was calculated separately for each class. This stratified analysis allowed the spatial agreement between each burned area product and the reference datasets to be evaluated under different land use and land cover contexts.

3.3. Low-Resolution Grid Regression Analysis

The assessment based on pixel-by-pixel confusion matrices was complemented by a regional accuracy analysis using linear regression metrics to analyze product limitations resulting from differences in spatial resolution between the evaluated burned area products and the higher-spatial-resolution reference datasets [13]. The proportion of burned area in each cell of a low-resolution grid was calculated for both the evaluated products (AQ1Km, FireCCIS311, MCD64A1, and VNP64A1) and the two reference datasets. A grid-cell size of 5 km $\times$ 5 km was used, which is larger than the native pixel size of the analyzed products but still small enough to reduce the spatial compensation of fires mapped in different locations within the same cell [10]. Scatter plots were constructed to compare the proportion of burned area detected by the products with the proportion mapped by the reference datasets. The RMSE was used to quantify the magnitude of differences between the burned area proportions estimated by each product and those mapped by the reference datasets, while the coefficient of determination (r^2) was used to express how much of the observed variability was explained by the linear relationship between the products and the references. RMSE values are expressed as percentage points of burned area proportion, representing the difference between the proportion of burned area estimated by each product and that mapped by the reference dataset in each grid cell. r^2 values close to 1 indicate high spatial consistency in the aggregated burned area proportions. This aggregated analysis was used as a complement to the pixel-based assessment because it reduces the effect of small spatial misalignments while preserving regional differences in burned area distribution.

3.4. Hit Probability Maps Based on Active Fire Hotspots

Kernel density-based spatial analysis was employed to investigate the relationship between pixels classified as TP in burned area products and the spatial distribution of active fire hotspots, allowing the identification of regions with greater spatial agreement with complementary active fire evidence and stronger spatial consistency with active fire occurrence. In the context of this study, hotspots provide complementary evidence of active fire occurrence and were used as a complementary spatial reference to evaluate the performance of the AQ1Km, FireCCIS311, MCD64A1, and VNP64A1 products. Because active fire hotspots indicate fire occurrence at the time of satellite overpass rather than the final burned extent, they were used as complementary evidence and not as a substitute for burned area reference maps. Georeferenced point data of active fire hotspots in shapefile format were obtained from the open data repository of the BDQueimadas Program (https://terrabrasilis.dpi.inpe.br/queimadas/bdqueimadas/, accessed on 2 April 2026) [53]. The hotspot dataset was filtered to match the same temporal window and spatial extent used for the burned area product assessment.

Kernel Density Estimation (KDE) is a non-parametric method used in this study to estimate the spatial distribution of point events, generating a continuous density surface from the location of active fire hotspots associated with TP pixels [54]. Active fire hotspots were associated with TP areas through direct spatial intersection. Specifically, hotspot points were overlaid with the TP polygons derived from the comparison between each burned area product and the reference datasets, and only hotspots located within TP polygons were retained for the subsequent KDE analysis.

The bandwidth was defined considering the spatial resolution of the products and the regional scale of fire scar propagation, seeking to balance spatial smoothing and preservation of local patterns. KDE was performed using a bandwidth of 1 km. The same bandwidth was applied to all burned area products to ensure comparability among density surfaces and to avoid introducing differences related to KDE parameterization. The selected bandwidth provided a balance between surface smoothness and the preservation of local hotspot concentration patterns. To this end, each active fire hotspot received a kernel smoothing function, whose contribution progressively decreases with distance from the central point. The sum of these contributions allowed the construction of spatial density maps capable of representing fire event concentration patterns. Therefore, a weighting function must be chosen to define how the influence of each hotspot decreases with distance. The quartic kernel function K(x) was adopted due to its ability to produce smooth surfaces without excessive loss of spatial detail, favoring the identification of heterogeneous clusters of active fire hotspots. The quartic method is based on the fourth-degree polynomial (Equation (3)):

$$K(x) = \frac{15}{16}\left(1 - x^2\right)^2 \quad (3)$$

where x represents the normalized distance within the kernel support, closely related to the bandwidth, with a value between -1 and 1. The function is 0 for values of x outside the support. The results were classified into quartiles, representing density gradients and allowing the identification of zones with low to high relative hit probability in fire detection. Thus, the term "hit probability" is used descriptively to represent the relative spatial concentration of hotspots associated with TP areas; it does not represent a probabilistic model of burned area occurrence. Based on the spatial overlap between the KDE-derived hit probability classes and the active fire hotspots, IoU and overall error (E) were calculated to quantify spatial agreement and detection deviations between the evaluated products. E was calculated as $E = 1 - OA$.

Importantly, the hotspot-based KDE analysis was not considered an independent validation of the burned area products, but rather a complementary assessment of their spatial consistency with active fire evidence. Active fire observations are used as auxiliary information in the generation algorithms of some of the evaluated products. However, the specific active fire observations effectively incorporated during the operational processing of each product were not available for this study, preventing a direct assessment of their spatial and temporal overlap with the BDQueimadas hotspot dataset. Therefore, potential dependence between these sources cannot be excluded, and KDE-derived agreement should be interpreted cautiously rather than as independent evidence of product accuracy.

4. Results

4.1. Photointerpretation Analysis

Figure 3 highlights marked differences between the burned area products and the GABAM and MapBiomas reference datasets, supported by Landsat color composite scenes, visually revealing distinct behaviors depending on the severity of the fire, the size of the polygons, the spatial heterogeneity, and the atmospheric limitations present in each region

of interest (ROI 1–6). The first column refers to Landsat 8/9 images, dated between August and October 2024, displayed as a false-color composite, with bands 5, 4, and 3 assigned to the red, green, and blue channels, respectively.

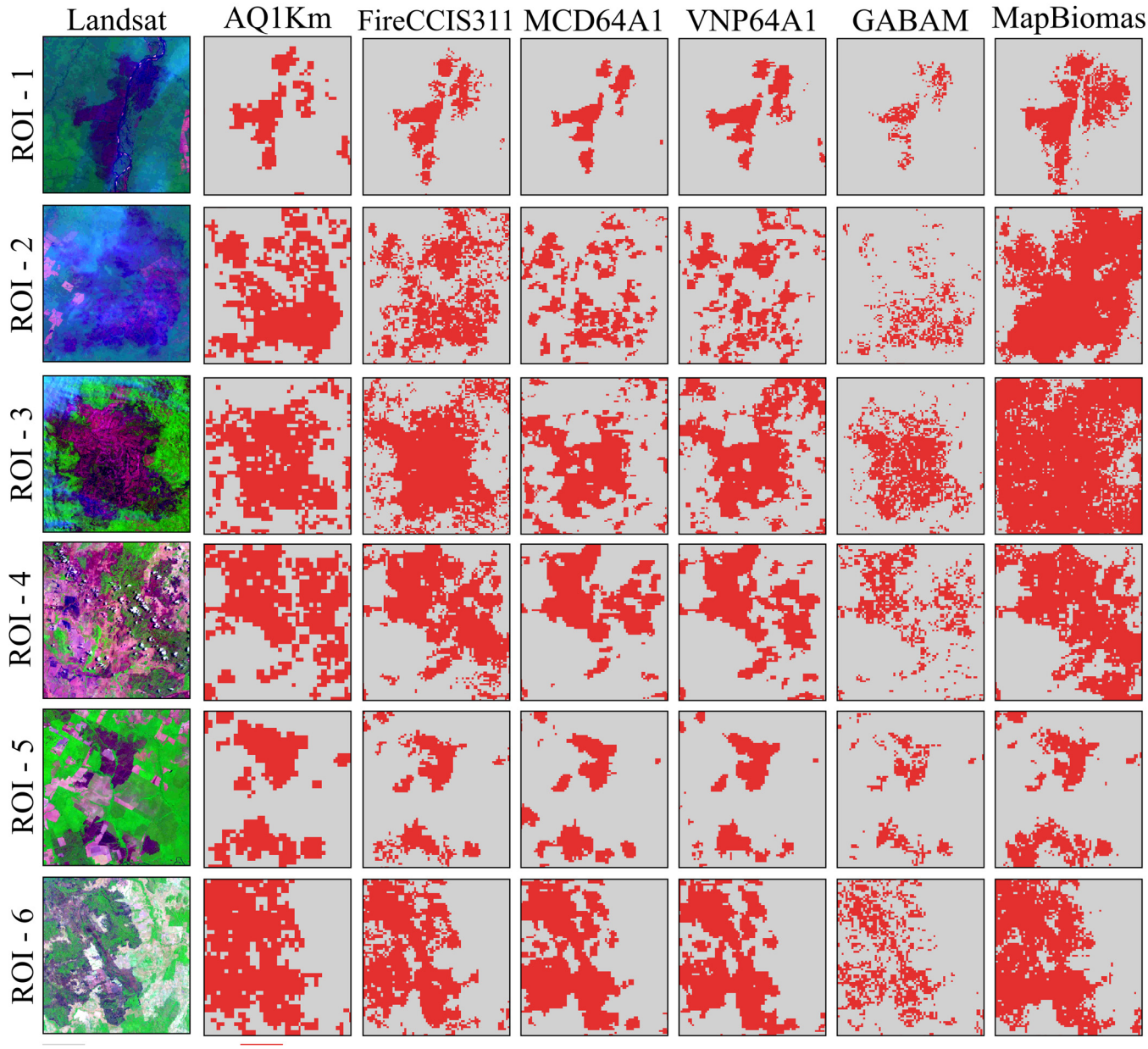


Figure 3. Comparison between burned area products and reference datasets across six regions of interest (ROIs) in the Xingu River basin. The first column displays Landsat 8/9 false-color composites (RGB: bands 5, 4, and 3) as visual support. In the burned area maps, red indicates pixels classified as burned, while light gray represents areas not classified as burned. The Landsat images used for this photointerpretation correspond to paths/rows 224/66 and 224/67, acquired on 2 September 2024.

Six regions of interest (ROIs) were used for visual inspection of the spatial correspondence among the burned area products, reference datasets, and Landsat imagery. The ROIs were selected for illustrative purposes and were not based on a formal statistical or stratified sampling design. Consequently, they were not intended to be spatially representative of the Xingu River basin or to contribute to the quantitative accuracy metrics. Rather, they were used to illustrate examples of spatial patterns and discrepancies observed during the visual comparison of the datasets.

A notable result of the photointerpretation is the spatial disparity between the two reference datasets themselves. GABAM and MapBiomas Fire show substantial differences in the extent, continuity, and fragmentation of mapped burned scars across several ROIs (Figure 3). In general, MapBiomas Fire depicts more spatially continuous burned areas in several examples, whereas GABAM frequently presents more fragmented patterns. These differences demonstrate that the reference datasets provide distinct representations of the same fire-affected landscapes. Consequently, disagreement between an evaluated product and a given reference cannot be interpreted independently of the uncertainty and mapping characteristics of that reference. The observed disparity therefore constitutes an important result of this study and provides direct evidence that the choice of reference dataset can influence the estimated commission, omission, and spatial agreement metrics.

In ROI 1, characterized by a compact burned scar with a strong presence of low-reflectance pixels, the products show good spatial coherence, but relevant differences in the estimated area. FireCCIS311 and MCD64A1 delineated wider and more continuous burned areas, visually closer to the reference datasets, although they show overestimation in some land cover contexts. In contrast, AQ1Km and VNP64A1 detect smaller areas, indicating partial omission at the edges of the burned scar. In ROI 2, the intense smoke contamination appears to reduce the spectral contrast between burned and unburned areas at the probable time of scene capture, compromising the performance of the algorithms. FireCCIS311 and MCD64A1 demonstrate high sensitivity, generating fragmented and potentially overestimated patterns. AQ1Km presents a more generalized response, with less spatial detail, while VNP64A1 maintains intermediate behavior, although still with notable omissions compared to GABAM and MapBiomas. In ROI 3, composed of an extensive, compact, and high-severity burned scar, greater convergence is observed between the products. FireCCIS311 and MCD64A1 adequately reproduce the main geometry of the burned polygon, although they enlarge peripheral areas. AQ1Km tends to smooth the boundaries due to its coarser spatial resolution, while VNP64A1 shows good spatial adherence, but with slight underestimation. It is important to emphasize that in this ROI, the temporal disparity between the annual products and the Landsat image may have had a stronger influence on the visual comparison.

In ROI 4, located within a mosaic of land use and land cover classes, the heterogeneity of the landscape makes it difficult to separate burned areas from naturally dark surfaces. FireCCIS311 and MCD64A1 incorporate adjacent areas, producing more continuous patches than the references. AQ1Km loses detail in smaller and narrower polygons, while VNP64A1 maintains greater selectivity, but with localized omissions. In ROI 5, formed by small isolated polygons, AQ1Km shows a strong detection limitation. FireCCIS311 and MCD64A1 identify parts of the areas, but frequently artificially enlarge the patches. VNP64A1 demonstrates a comparatively greater ability to detect smaller fragments. In ROI 6, associated with low-severity fires, there is greater divergence among the products. FireCCIS311 and MCD64A1 detect larger areas, with a risk of overestimation, while AQ1Km shows substantial omissions, and VNP64A1 identifies only the most intensely burned portions. In general, the AQ1Km, FireCCIS311, MCD64A1, and VNP64A1 products respond in a moderately similar manner to the spectral and spatial characteristics of burned scars, with clear tendencies of overestimation or underestimation in relation to the reference datasets. On the other hand, FireCCIS311 tends to show greater sensitivity to burned area detection, frequently resulting in spatial overestimation, while AQ1Km, MCD64A1, and VNP64A1 show more selective behavior, with a higher probability of omission.

4.2. Spatial Distribution of Detection Errors and Shape Index Analysis

Figure 4 presents the spatial distribution of classification outcomes (TN, FP, FN, and TP) and the geometric complexity of burned scars (Shape Index) for the products AQ1Km, FireCCIS311, MCD64A1, and VNP64A1, using the MapBiomas and GABAM datasets as references. In general, true negatives (TN) predominate in all products, reflecting the large extent of unburned areas in the study region. However, the differences between the products become evident in the proportion and spatial distribution of FP, FN, and TP.

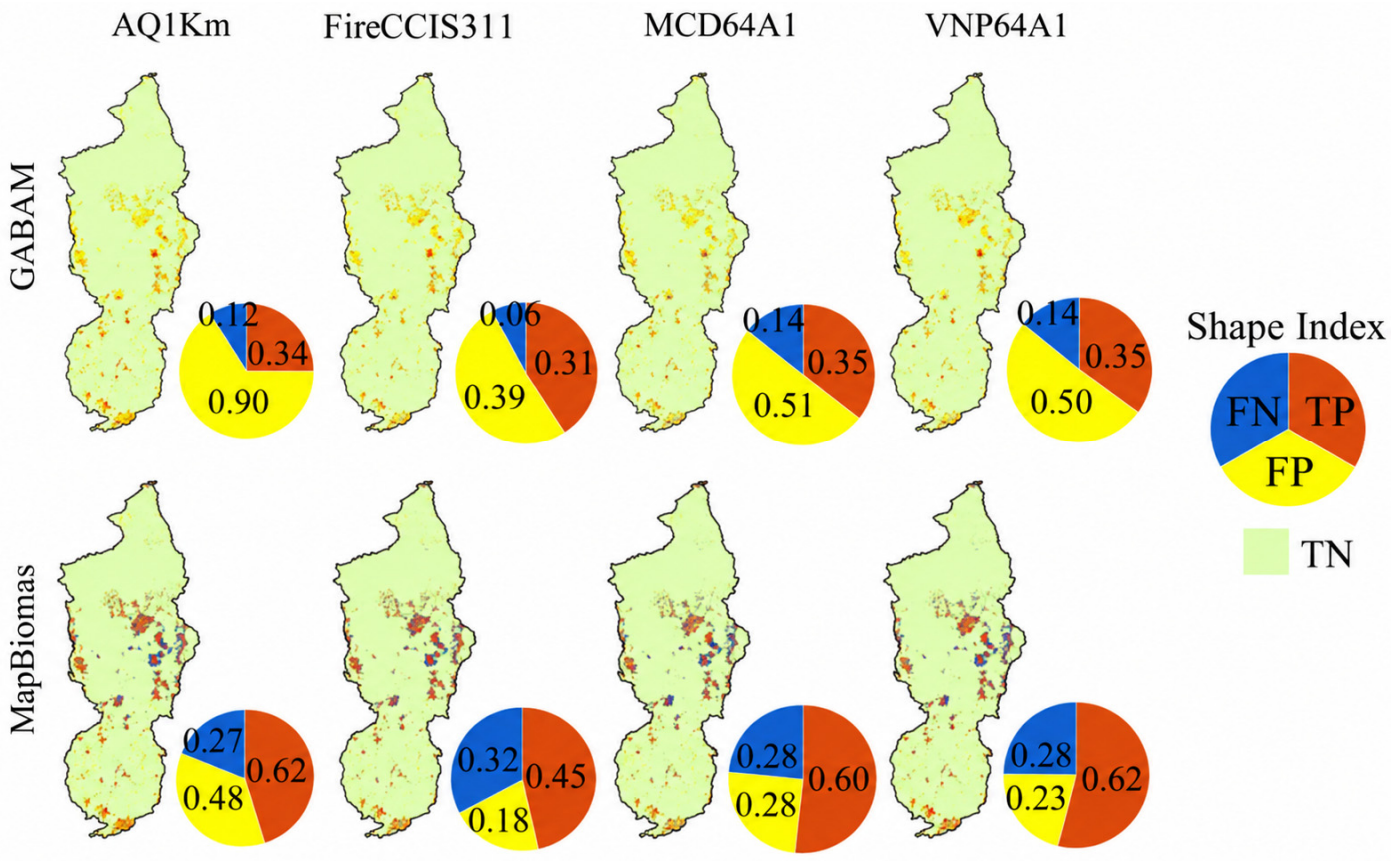


Figure 4. Spatial distribution of burned area classification outcomes and Shape Index values for the evaluated products compared with MapBiomas and GABAM.

When GABAM is used as reference, FP is particularly extensive for AQ1Km (3.50×10^4 km^2) and FireCCIS311 (2.30×10^4 km^2), indicating substantial disagreement between product-detected burned areas and GABAM. The Shape Index also shows distinct FP patterns, with values of 0.90, 0.39, 0.51, and 0.50 for AQ1Km, FireCCIS311, MCD64A1, and VNP64A1, respectively. FN is comparatively relevant for VNP64A1 (3.41×10^3 km^2), while TP remains below 1×10^4 km^2 for all products, indicating limited spatial correspondence with GABAM. In contrast, comparison with MapBiomas shows lower FP and FN and greater TP. FireCCIS311 presents the lowest FP (7.03×10^3 km^2), whereas AQ1Km has the highest TP (2.66×10^4 km^2), despite higher FP than the other products. MCD64A1 and VNP64A1 show intermediate patterns. Overall, the greater TP and reduced disagreement observed against MapBiomas demonstrate that classification outcomes are strongly dependent on the reference dataset, reinforcing the need to interpret FP and FN relative to each reference rather than solely as product-specific errors.

The Shape Index analysis reveals clear differences among the products in the representation of the geometric complexity of classification outcomes, with distinct patterns depending on the reference dataset used. In relation to MapBiomas, AQ1Km presents

high Shape Index values for FP, indicating more irregular and fragmented patches, which reinforces its tendency to overestimate burned areas. FireCCIS311, in turn, presents FP with lower relative complexity and more consistent values for TP, indicating a better representation of burned scar geometry. The MCD64A1 and VNP64A1 products exhibit intermediate behavior, with FP still complex but less irregular than in AQ1Km, and TP showing partially preserved geometry. In all products, FN present lower complexity, mainly associated with the omission of smaller and more regular areas.

Regarding GABAM, a distinct pattern is observed, marked by the predominance of FP in all products. In this context, the high Shape Index values for FP largely reflect the generalized overestimation of burned areas, limiting the interpretation of geometric complexity as a direct representation of actual burned scar geometry. AQ1Km presents the most irregular FP, while FireCCIS311, MCD64A1, and VNP64A1 maintain similar patterns, although still influenced by over-detection. TP shows less geometric consistency compared to MapBiomas, reflecting the lower spatial agreement observed in the IoU analysis. Spatially, the concentration of FP and FN in the central and southern regions of the basin reinforces the influence of landscape heterogeneity on error generation. In summary, FireCCIS311 presents better geometric precision compared to MapBiomas, while AQ1Km stands out for its greater sensitivity, but also greater spatial irregularity of errors, a pattern that intensifies when evaluated against GABAM. In this context, the inherent complexity of burned area detection imposes relevant limitations on mapping. One of the main associated factors is the heterogeneity and fragmentation of the Amazonian landscape. As discussed by Shimabukuro et al. [55], the coexistence of different land use and land cover classes, coupled with the diversity of Amazonian vegetation patterns, requires an understanding of how these elements influence burned area detection, especially in tropical regions, where complex mosaics and accelerated landscape dynamics predominate. These patterns indicate that mapping uncertainty is spatially uneven and partly associated with the territorial heterogeneity of the basin.

4.3. Accuracy Metrics

Figure 5 presents a comparison of the performance of the AQ1Km, FireCCIS311, MCD64A1, and VNP64A1 products based on the OA, CE, IoU, and OE metrics, considering the MapBiomas and GABAM datasets as references. In general, when compared to GABAM, the analyzed products showed high CE. However, when compared to MapBiomas, the CE and OE were more balanced, without large differences among products. This behavior is common in analyses involving products and reference data obtained at different spatial resolutions, where the size and irregularity of burned targets can directly influence error rates [56].

Regarding MapBiomas, a greater balance is observed among the products. FireCCIS311 presents the best overall performance, with the highest IoU (52.67%) and low CE (21.83%), although still with moderate OE (38.25%). AQ1Km also stands out, with an IoU of 45.44% and the lowest OE (34.78%), indicating good detection capability, but with a higher CE (40.03%). MCD64A1 and VNP64A1, on the other hand, show higher OE (~50%), which negatively impacts their IoU values (41.09% and 44.23%, respectively), indicating a substantial loss of burned areas, despite relatively moderate CE. When compared to GABAM, all products show a sharp drop in performance, especially in IoU (20%–27%). The main factor associated with this reduction is the marked increase in CE, which exceeds 69% in all products, indicating a strong tendency to overestimate burned areas. On the other hand, OE values are relatively low (16%–30%), suggesting that the products are able to identify a large part of the burned areas mapped by GABAM, but with low spatial agreement.

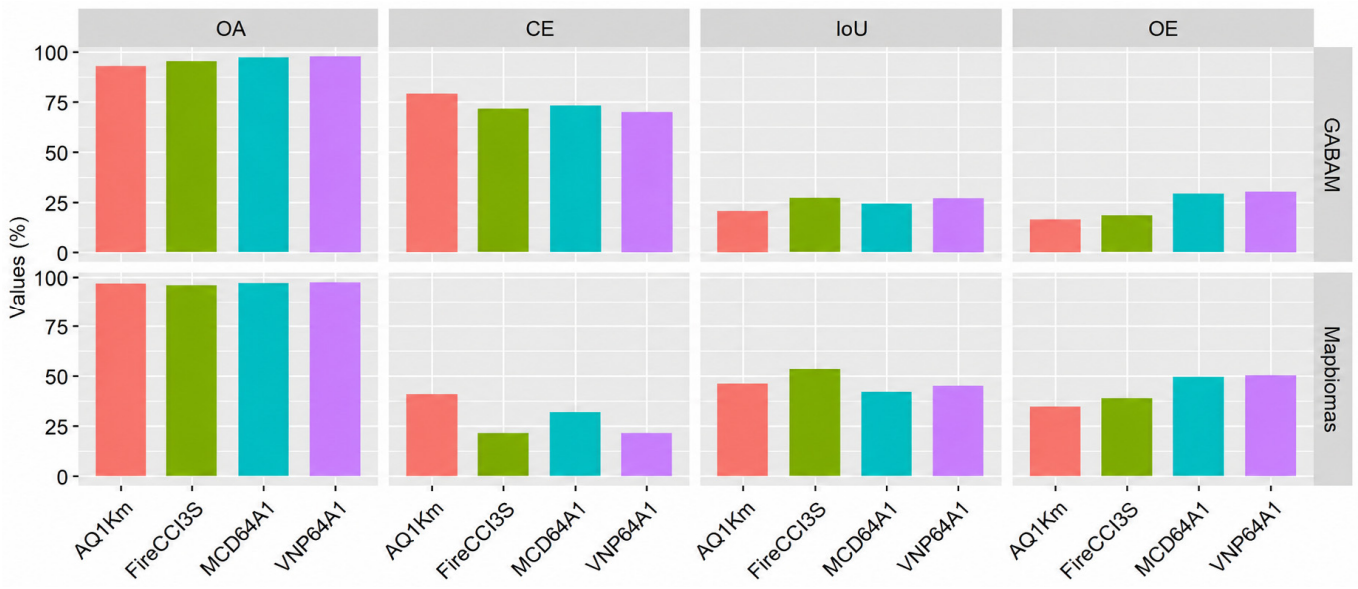


Figure 5. Accuracy metrics for the products AQ1Km, FireCCIS311, MCD64A1, and VNP64A1 in relation to the MapBiomas and GABAM reference datasets.

These results, especially when compared with MapBiomas, are consistent with the findings of Giglio et al. [13]. The authors reported, for tropical forests, OE values around 59% and CE of approximately 29% for the MCD64A1 and VNP64A1 products, with OA exceeding 98%. Globally, however, the same authors observed that VNP64A1 consistently maps a slightly larger burned area than that detected by MCD64A1, with a relative surplus ranging from 2.1% (2017) to 6.3% (2013). In the overall analysis, the OE and CE values were 72.4% and 36.7%, respectively, which corroborates the error patterns observed in the present study. Consistent with the results of this study, Ouattara et al. [57], Matveev et al. [23], and Bastarrika et al. [8] report a predominance of high OE in the MCD64A1 and VNP64A1 products, frequently in the range of 60%–75% globally or in challenging biomes, with moderate CE, typically 30%–40%. FireCCI tends to show greater sensitivity, with lower OE than MODIS/VIIRS products in several contexts, but with slightly higher CE in some cases, aligning with the spatial overestimation trend observed in this study. For example, in validations conducted in Russia, Matveev et al. [23] showed that FireCCI products had better OA than MCD64A1 and VNP64A1, which exhibited high OE values (~60%–70%). Similar patterns of high OE and variable CE have also been reported in cropland and Mediterranean studies. These similarities reinforce the inherent limitations of moderate-resolution sensors and algorithms in complex biomes, with better performance in large and compact fires and greater discrepancies against high-resolution references, as discussed in this study. The integration of active fire data, as in AQ1Km and VNP64A1, helps improve sensitivity but does not completely eliminate the trade-offs between OE and CE [13,58].

In general, all products exhibit high OA against both reference datasets (>92%). Among the products, FireCCIS311 and VNP64A1 show the highest IoU against GABAM (26.95% and 26.76%, respectively). AQ1Km shows the lowest IoU (20.46%), associated with the highest CE (78.71%), indicating strong overestimation. MCD64A1 shows intermediate performance, with the highest OA (97.14%), but still with important limitations in spatial correspondence. Complementing the accuracy analysis, Figure 6 highlights the influence of burned scar size on product performance based on the IoU metric. In that sense, Figure 6 shows that all products have poor performance for very small scars (0–5 km^2), while IoU generally increases with scar size, although some products show a decrease for very large scars (>75 km^2).

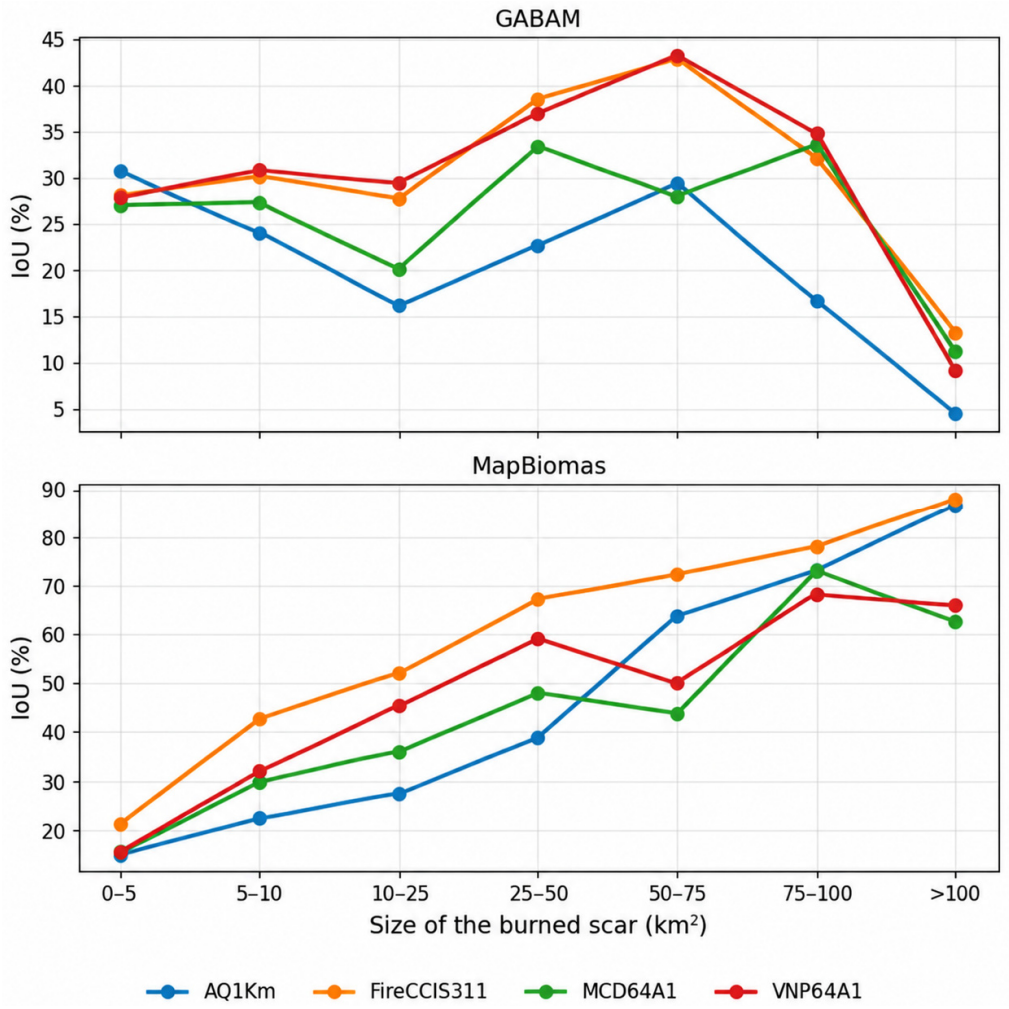


Figure 6. Comparison of product IoU across burned area size classes.

For GABAM, IoU values are relatively low across all size classes, ranging approximately from 10% to 45%. There is a slight improvement in performance for intermediate scars (25–75 km^2), especially for FireCCIS311 and VNP64A1, which achieve the highest values (~40%–45%). However, for very large scars (>100 km^2), all products show a sharp drop in IoU, particularly AQ1Km, which reaches the lowest values. This behavior suggests limitations in spatial matching in large-scale events, possibly associated with edge overestimation or spatial displacements relative to the high-spatial-resolution reference data. In contrast, for MapBiomas, a more consistent and increasing pattern is observed: IoU increases progressively with the size of the burned scars. For small areas (0–5 km^2), the values are low (~15%–20%), indicating widespread difficulty in detecting small-scale fires. As size increases, there is a substantial performance gain, with IoU values exceeding 70% for scars larger than 75 km^2 and reaching up to ~85% for AQ1Km and FireCCIS311 in areas > 100 km^2. Among the products, FireCCIS311 shows superior and more consistent performance across size classes, especially against MapBiomas, while AQ1Km tends to show greater variability and lower performance in small and very large scars when evaluated against GABAM. MCD64A1 and VNP64A1 show intermediate behavior, with gradual improvements as a function of increasing scar size.

The contrasting patch size patterns obtained with the two reference datasets should also be interpreted in relation to their spatial structure. The greater fragmentation and occurrence of unburned gaps within burned complexes mapped by GABAM may reduce spatial correspondence with the 300–1000 m products even for large patches, because coarse

pixels cannot reproduce fine-scale internal heterogeneity. This may partly explain why IoU does not increase consistently with patch size against GABAM, unlike the clearer size-dependent pattern observed with MapBiomas Fire. In Amazonian forests, low-intensity understory fires beneath closed canopies may also produce spatially heterogeneous spectral responses and discontinuous detection. However, the present analysis cannot distinguish whether the finer fragmentation observed in GABAM reflects actual within-scar heterogeneity or differences arising from its mapping framework. Thus, both landscape-scale fire characteristics and reference dataset structure should be considered when interpreting patch-size-dependent agreement.

Thus, even with the useful performance patterns observed for the analyzed products, limitations persist regarding their ability to adequately represent burned areas under different land cover contexts. To investigate this aspect, the MapBiomas LULC dataset (30 m) was used to evaluate product performance by thematic class. Table 2 shows the IoU values obtained by each product in relation to the reference data, considering the spatial intersection with the different land use and land cover classes, allowing for a more detailed analysis of the influence of landscape context on mapping accuracy. Considering the five predominant LULC classes included in the stratified analysis and normalizing their areas to the total analyzed basin area (531,250 km^2), Forest Formation represents approximately 390,949 km^2, Savanna Formation 10,924 km^2, Forestry 119,776 km^2, Flooded Forest 8490 km^2, and Pasture 1111 km^2.

Table 2. IoU values by land use and land cover class for each burned area product (G: GABAM, M: MapBiomas). The classes represent distinct ecological and land management contexts within the basin.

LULC	AQ1Km		FireCCIS311		MCD64A1		VNP64A1	
	G	M	G	M	G	M	G	M
Forest Formation	0.14	0.45	0.16	0.48	0.18	0.41	0.18	0.43
Savanna Formation	0.33	0.61	0.40	0.64	0.40	0.55	0.40	0.55
Forestry	0.45	0.44	0.58	0.51	0.55	0.54	0.27	0.20
Flooded Forest	0.22	0.37	0.31	0.41	0.27	0.34	0.27	0.34
Pasture	0.27	0.46	0.40	0.58	0.37	0.45	0.38	0.46

Regarding GABAM, IoU values are generally lower than those obtained with MapBiomas across the LULC classes. Forestry represents a notable exception, with higher IoU values against GABAM for all four products (VNP64A1: 0.27 vs. 0.20; MCD64A1: 0.55 vs. 0.54; FireCCIS311: 0.58 vs. 0.51; AQ1Km: 0.45 vs. 0.44). FireCCIS311 shows the highest IoU against GABAM in Forestry (0.58), followed by MCD64A1 (0.55). Even so, FireCCIS311 shows the best results in most classes, particularly in forestry (0.58), pasture (0.40), and savanna formation (0.40). MCD64A1 and VNP64A1 show similar performance in some classes, such as forest and savanna formation, but with less overall consistency. AQ1Km generally shows the lowest values, indicating limitations in detailed spatial representation. For MapBiomas, the IoU values are markedly higher, confirming greater compatibility between the products and this reference. Again, FireCCIS311 stands out, presenting the highest values in almost all classes, such as savanna formation (0.64) and pasture (0.58). MCD64A1 shows competitive performance in forestry (0.54), surpassing the others in this specific class. VNP64A1 shows intermediate behavior, while AQ1Km maintains relatively lower performance.

In general, classes such as savanna formations and pasture show the highest IoU values, indicating that these environments favor detection by the products, possibly due to lower vegetation density, greater burned scar continuity, and greater spectral contrast after burning. In contrast, forest formations and flooded forests show intermediate performance,

reflecting limitations associated with closed canopy, shading, and the occurrence of understory fires, which reduce detectability. The products therefore did not provide equally reliable spatial evidence across the land use mosaic, with lower agreement in forested settings than in savanna formations and pasture.

4.4. Low-Resolution Regression Metrics

The confusion matrices and derived accuracy metrics were complemented by low-resolution regression metrics, based on comparing the proportion of 5 km × 5 km cells detected as burned by AQ1Km, FireCCIS311, MCD64A1, and VNP64A1 with the proportion mapped as burned in the independent reference datasets from MapBiomas and GABAM (Figure 7). The regression plots highlight the relationship between the proportion of burned area estimated by the products and the reference datasets, allowing for a more in-depth interpretation of the accuracy and IoU results previously discussed.

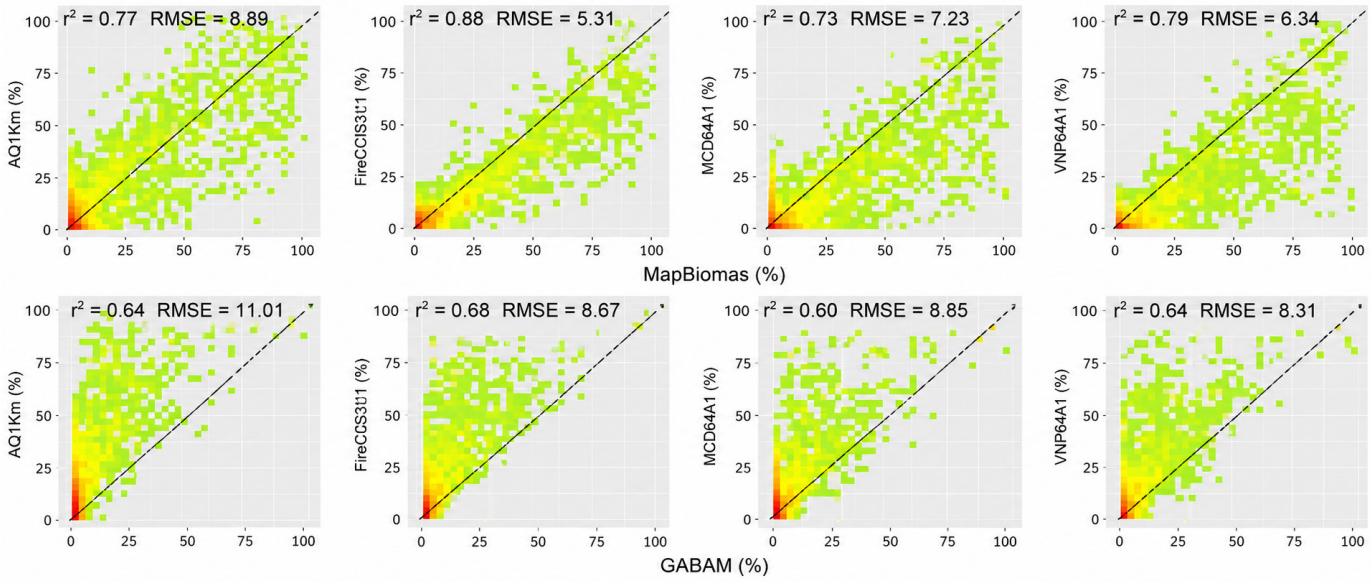


Figure 7. Scatter plots of burned area proportions within 5 km × 5 km grid cells classified as burned by the evaluated products versus the reference datasets. RMSE values are expressed in percentage points of burned area proportion.

Regarding MapBiomas, a strong linear relationship is observed for all products, with high coefficients of determination (r^2 between 0.73 and 0.88). FireCCIS311 shows the best performance (r^2 = 0.88; RMSE = 5.31 percentage points), indicating greater consistency in estimating the proportion of burned area. VNP64A1 (r^2 = 0.79; RMSE = 6.34 percentage points) and AQ1Km (r^2 = 0.77; RMSE = 8.89 percentage points) also demonstrate good agreement, while MCD64A1 shows greater dispersion (r^2 = 0.73; RMSE = 7.23 percentage points). These results are consistent with the IoU analysis shown in Figure 5, in which FireCCIS311 showed better overall performance, especially for larger burned scars, reflecting a greater ability to reproduce spatial patterns mapped by MapBiomas. In contrast, regarding GABAM, there is a marked reduction in the linear relationship (r^2 between 0.60 and 0.68) and an increase in errors (RMSE between 8.31 and 11.01 percentage points), highlighting a greater discrepancy between the products and this higher-spatial-resolution reference. AQ1Km presents the highest error (RMSE = 11.01 percentage points), while FireCCIS311, MCD64A1, and VNP64A1 maintain similar but still limited performance. The more pronounced dispersion and the concentration of points close to low reference values indicate difficulties in representing small and fragmented burned areas, corroborating the more pronounced areas of FN and FP observed for GABAM in Figure 4.

Previous studies show that, for MCD64A1, the results of the present study are close to those obtained by Giglio et al. [11], Boschetti et al. [12], and Giglio et al. [13], who reported linear agreement values of 0.88, 0.74, and 0.70, respectively. However, they differ from Pereira et al. [59], who reported a slightly lower value (0.57). On the other hand, Silva Júnior et al. [58] obtained a correlation of 0.57 and an RMSE of 1.63 percentage points for the AQ1Km product, values that diverge from the results of the present study. Pereira et al. [59] reported a correlation of 0.71 for AQM-PROBA, a value closer to that found in this work. Long et al. [46], in turn, obtained an intermediate correlation of 0.74 for the previous version of FireCCI, which can still be considered a good result.

4.5. Active Fire Hotspot Density and Hit Probability Analysis

Spatial analysis using KDE of active fire hotspots associated with pixels classified as TP reveals consistent patterns of agreement between burned area products and complementary evidence of active fire occurrence. Density maps, interpreted here as hit probability maps, highlight regions of greater alignment between burned scar detection and active fire occurrence, with gradients ranging from blue (low density/probability) to red (high hit probability) (Figure 8). In general, spatial patterns are consistent across products, with hotspots concentrated in the south-central portion of the study area, indicating regions of higher hotspot concentration and better detection. However, the intensity and extent of these areas vary markedly, reflecting the balance between omission and commission already observed in accuracy and IoU analyses.

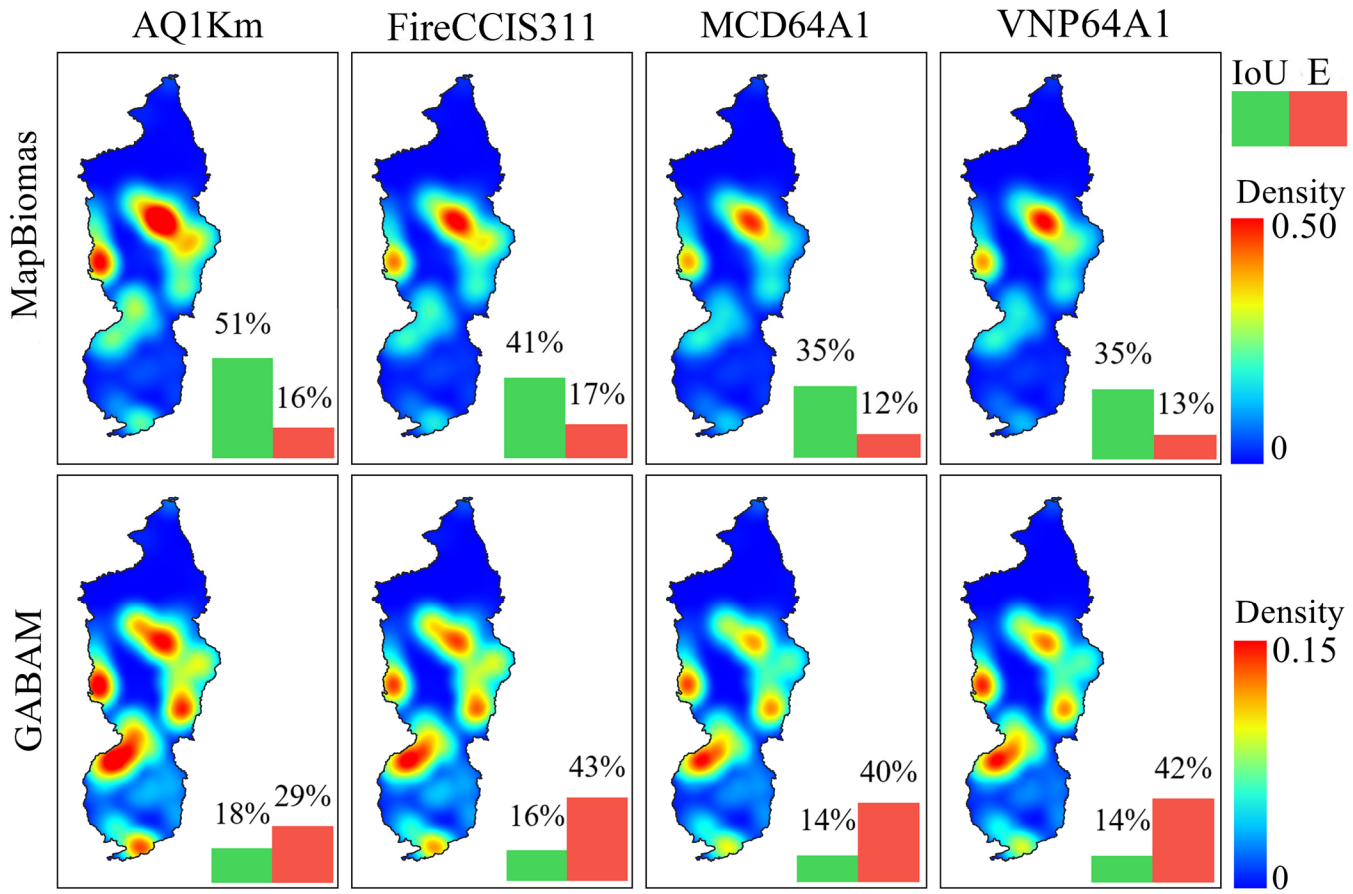


Figure 8. Active fire hotspot density associated with TP areas for each burned area product. The density surfaces represent relative spatial concentration rather than modeled probabilities of wildfire occurrence. Note that the MapBiomas Fire and GABAM rows use different density scales to preserve within-reference spatial contrast; colors should therefore not be compared quantitatively between rows.

FireCCIS311 stands out as the product with the best overall performance in this hit probability approach. Its maps show more continuous and spatially coherent high-density cores, indicating greater alignment between TP areas and active fire hotspots. Despite a slight expansion of these areas, the product maintains good spatial consistency, which is corroborated by the higher IoU (52.67% with MapBiomas) shown in Figure 5 and the better regression performance (r^2 = 0.88) shown in Figure 7. This combination suggests that FireCCIS311 balances sensitivity and precision, adequately capturing the spatial distribution of burned areas, especially in medium- to large-scale events.

The AQ1Km exhibits the highest maximum density values and the largest hotspot coverage area, indicating high sensitivity to fire detection. This translates into a higher hit probability in regions with a high concentration of active fires (51%), but is accompanied by a higher E of 16%. This pattern reinforces previous results: the product detects more burned areas, resulting in lower omission, but tends to spatially overestimate (CE ~40% against MapBiomas), diluting spatial precision. Thus, its high density does not necessarily represent better accuracy, but rather a greater inclusion of potentially burned areas. The MCD64A1 and VNP64A1 products exhibit intermediate and relatively similar behavior. Both show more compact and less intense density cores, indicating greater selectivity in detection. This results in lower E rates (12%–13%), but also in lower coverage of active fire hotspots (IoU ~35%). This pattern is aligned with the higher OE (~50%) observed in the accuracy analysis, suggesting that these products tend to detect only the most evident portions of burned scars, especially in areas likely associated with greater fire severity.

When GABAM is used as reference, FP is particularly extensive for AQ1Km (3.50×10^4 km^2) and FireCCIS311 (2.30×10^4 km^2). The normalized shape-compactness values for FP are 0.90, 0.39, 0.51, and 0.50 for AQ1Km, FireCCIS311, MCD64A1, and VNP64A1, respectively. These values indicate differences in the spatial compactness of FP patterns, with AQ1Km showing a comparatively more compact configuration and FireCCIS311 a less compact and more irregular configuration, while MCD64A1 and VNP64A1 present intermediate and similar patterns. In the analysis based on GABAM, a marked reduction in IoU values is observed, accompanied by an increase in the overall error (E) and relative hotspot, consistent with previous results. AQ1Km stands out by presenting the highest hit probability values, evidenced by the more intense cores (red tones). On the other hand, MCD64A1, VNP64A1, and FireCCIS311 exhibit relatively balanced IoU and E values, but with slightly lower hit probability values. This superior performance of AQ1Km in the hotspot density analysis may be associated with its methodological approach, which explicitly incorporates active fire hotspot data into the detection process. This integration tends to increase spatial convergence with areas classified as TP, consequently resulting in higher hit probability values in the density maps.

5. Discussion

The analysis of the results reveals that the performance of burned area products (AQ1Km, FireCCIS311, MCD64A1, and VNP64A1) in the Xingu River basin is directly influenced by several factors, including spatial and temporal resolution, sensor characteristics, environmental conditions, landscape heterogeneity, and algorithm design. Although isolating the impact of each factor remains challenging, the combined analyses provide important information about their relative influence on burned area detection. The discrepancies observed in this work are consistent with recent studies by Padilla et al. [60], Giglio et al. [13], Liu et al. [6], and Bastarrika et al. [8], reinforcing the need for caution when interpreting global metrics, especially in complex tropical regions, and the need to use reference data appropriate to the heterogeneity of the Amazonian landscape. In the context of increasing drought frequency, climate-related fire susceptibility, and an-

thropogenic pressure, the improvement and quality assessment of these remote sensing products are essential to support policies for fire prevention, fire control, risk management, and biodiversity conservation in the Xingu River basin and throughout the Amazon [61].

The implications of these discrepancies extend beyond remote sensing product assessment. In the Xingu basin, conservation units, Indigenous Lands, forest formations, and agricultural frontiers coexist within a shared fire-prone landscape. The spatial reliability of burned area information therefore affects the evidence available for wildfire surveillance, impact assessment, conservation planning, and territorial decision-making.

5.1. Influence of Burned Scar Shape, Size, and LULC on the Accuracy of Burned Area Products

The results obtained show that the performance of burned area products varies substantially depending on the spatial resolution, the detection methodology employed, the size and geometry of the burned scars, and the reference dataset used [62]. Overall, the four products analyzed (AQ1Km, FireCCIS311, MCD64A1, and VNP64A1) showed OA above 90%, but with contrasting patterns of CE and OE. This contrast reinforces the need for caution when selecting burned area products and reference data, since the choice of reference dataset has a substantial influence on the assessment of accuracy and spatial representation of burned scars. Because OA is strongly affected by the dominance of unburned pixels, the interpretation of product performance should rely primarily on CE, OE, IoU, and spatial agreement metrics. Additionally, differences in the definition of "burned area" among algorithms, especially regarding the inclusion of edges and partially burned pixels, may explain some of the discrepancies. In this context, studies by Boschetti et al. [45], Oliveira and Sehn Körting [5], Chuvieco et al. [7], and Valencia et al. [28] highlight that differences in spatial resolution can produce edge shifts and spatial compensation effects, potentially increasing CE and OE in pixel-by-pixel comparisons. Thus, some of the observed discrepancies do not necessarily represent absolute failures of the products, but rather limitations inherent to the spatial scale of the sensors originally used. The stronger hotspot-based spatial agreement observed for some products should also be interpreted considering their algorithmic design, since active fire observations are incorporated as auxiliary information in burned area detection. Therefore, part of the observed agreement may reflect this methodological dependence rather than solely superior burned scar detection performance.

The Shape Index analysis reinforces this interpretation by demonstrating that classification outcomes are associated not only with the amount of area detected, but also with the geometric complexity of the burned scars. AQ1Km showed more irregular and fragmented false positives, while FireCCIS311 showed greater preservation of the burned scar geometry. In all products, false negatives tended to show more compact shapes and smaller dimensions, suggesting that small and spatially isolated burned areas remain the main challenge for detection algorithms. This pattern is likely related to the heterogeneity of the Amazonian landscape, where mosaics of forest, pasture, agriculture, and secondary vegetation hinder the spectral separation between burned areas and naturally dark surfaces [55,63]. Savanna formations and pastures presented the highest IoU values (up to 0.72 in MapBiomas), possibly indicating that environments with more open vegetation and greater post-fire spectral contrast favor detection. Similarly, Ramos et al. [9] reported the highest accuracy for tropical and savanna formations in the Amazon, although direct comparisons are complicated by methodological differences, particularly the use of Landsat spectral index thresholds. The authors emphasize that the detection of burned areas in forest regions is generally more prone to OE, and even high-resolution products showed limited performance. On the other hand, forest formations and flooded forests exhibited intermediate performance, likely because of closed canopy conditions, the occurrence of understory fires, and shading [10,64,65]. FireCCIS311 showed the best performance, which

may be related to its Sentinel-3-based spatial resolution (300 m) compared to the other products with coarser pixel sizes (500–1000 m). This pattern is widely documented in the literature and reflects limitations inherent to the moderate- to coarse-spatial-resolution sensors, which are affected by spectral mixing in pixels containing burned area edges or fragments [6,13,20,23,52,58,59].

From a landscape perspective, these results indicate that mapping uncertainty is partly structured by the spatial configuration of the vegetation and land cover mosaic. Land use change and fragmentation modify the spectral and geometric conditions under which burned areas are observed, leading to different levels of mapping agreement among forest, savanna, forestry, flooded-forest, and pasture environments.

5.2. General Analysis of Product Accuracy

Overall, FireCCIS311 presented the best balance between sensitivity and accuracy, especially when compared against MapBiomas Fire, achieving the highest IoU (52.67%) and the best fit in the 5 km grid regression (r^2 = 0.88). Its higher spatial resolution (300 m) compared to other evaluated products and the integration of Sentinel-3 data with active fire information from VIIRS increase its ability to detect complex and fragmented burned scars, which are common in the Amazonian landscape [18]. According to Stroppiana et al. [24] and Katagis and Gitas [56], FireCCI51 products tend to show good spatial agreement with high-spatial-resolution references in several biomes and lower overall bias in some regions. However, FireCCI51 products may also present higher CE in some cases, reflecting the trade-off between sensitivity and spatial precision. It is important to note that FireCCIS311 and FireCCI51 are different versions within the FireCCI product family. Therefore, these comparisons aim to highlight general performance patterns across the FireCCI family, and not a direct equivalence between the products. These results corroborate previous studies that indicate greater sensitivity of FireCCI compared to traditional MODIS- and VIIRS-based products. Padilla et al. [17] reported global Dice indices of approximately 45% for MCD64 and about 56% for FireCCIS311. Stroppiana et al. [24], in their study in Africa, showed that among the coarse-spatial-resolution products, FireCCIS311 presented the best overall results, with Dice coefficients of 67.3% for small areas and 64.4% for mosaic areas, surpassing FireCCI51 and MCD64, which exhibited substantially higher OE. Spatial resolution has also been identified as a key source of error, contributing to CE due to partially burned pixels and OE due to undetected small burns [15].

The observed behavior for AQ1Km reinforces this trade-off between sensitivity and spatial accuracy. The product showed considerable detection capability, reflected in the smaller OE; however, it also exhibited the largest CE and the highest Shape Index values for false positives, indicating a tendency toward overestimation and the generation of spatially irregular patches, a pattern that may be related to its coarser spatial resolution [20,58,59]. Despite this, this behavior suggests that integrating national active fire hotspot data into the algorithm may increase the ability to identify fire events, as observed in the higher hit probability values associated with active fires shown in the maps of Figure 8. Silva Junior et al. [58] showed that AQ1Km obtained good spatial correlation in a transition basin between the Cerrado and Amazon biomes when analyzed on an aggregated 10 km × 10 km grid, with reduced pixel dispersion, burned area proportions above ~30%–40%, and r^2 values above 0.40 in 2022 and 2023, presenting metrics comparable to those obtained from supervised mapping using 64 m multispectral images. Libonati et al. [20] highlight that MCD64A1 uses an algorithm based on global generalizations, whereas AQ1Km is based on a regional algorithm, calibrated for Brazilian biomes. In their analyses, MCD64A1 underestimated total burned area by an average factor of 2.4, while AQ1Km estimated values 1.3 times greater than those derived from 30 m reference images

during the validation periods. Thus, despite its 1 km spatial resolution and coarser pixel size compared to the other evaluated products, the results of this study demonstrate that regionally adapted burned area detection algorithms, such as AQ1Km, can still perform competitively with global products, especially in terms of sensitivity, burned scar size analysis, and convergence with active fire hotspots.

In this study, the MCD64A1 and VNP64A1 products showed intermediate behavior, characterized by greater spatial selectivity and lower E values in some analyses, but accompanied by high OE. These values are similar to those reported by Giglio et al. [13] for tropical forests (OE ~59% and CE ~29%). Similarly, Matveev et al. [23] observed OE of approximately 60%–70%, while Román et al. [25] reported CE of about 36.7% for VNP64A1 and 34.2% for MCD64A1, in addition to OE of approximately 72.4% and 71.5%, respectively. In this sense, Giglio et al. [13], Bastarrika et al. [8], and Matveev et al. [23] report difficulties with the MCD64A1 and VNP64A1 products in detecting small, low-severity fires or fires under dense forest cover. According to Parente et al. [29], Franquesa et al. [54] and Pacheco et al. [26], the dependence on relatively intense spectral changes in SWIR and NIR means that these algorithms perform well in extensive and homogeneous fires, but have limitations in fragmented events or those partially obscured by the canopy. In the Amazon, this limitation becomes particularly relevant due to the high occurrence of understory fires and low-intensity fires, whose spectral signature can be confused with shadows, surface moisture, or forest degradation [10,33,35,55,66].

These contrasts indicate that product selection should be purpose-specific. FireCCIS311 is better suited to applications that prioritize spatial agreement and geometric fidelity, whereas AQ1Km may be useful when maximizing sensitivity is more important than minimizing false detections. MCD64A1 and VNP64A1 retain value for consistent large-area monitoring, but their omission of small and fragmented burns should be recognized when the products are used to support territorial assessments and wildfire management activities.

5.3. Sensitivity to the Validation Framework: MapBiomas vs. GABAM

The choice of reference data also strongly influenced the results, evidenced by the divergence in product performance when compared against different higher-spatial-resolution (30 m) reference datasets. The markedly greater agreement with MapBiomas Fire (Collection 4) compared to GABAM suggests that MapBiomas, as a regionally calibrated product for Brazilian biomes, may capture vegetation and fire regime characteristics of the Amazon that global reference products may overlook. When compared to MapBiomas Fire, the products showed more balanced errors and markedly higher IoU values, especially for FireCCIS311 (IoU = 52.67%) and AQ1Km (IoU = 45.44%). In contrast, validation with GABAM, also at 30 m but based on an automated global approach, resulted in a sharp drop in IoU (20%–27%) and a marked increase in CE (>69%) for all products. The high CE values observed in relation to GABAM (>69% for all products) indicate that this reference dataset may omit some burned scars detected by moderate-resolution products, or that methodological incompatibilities between algorithms affect the comparison. Alternatively, part of this pattern may also reflect overestimation by the evaluated products, particularly in heterogeneous landscapes where burned and unburned surfaces are spectrally mixed. This divergence reinforces the recommendations of Boschetti et al. [45] and Chuvieco et al. [7] regarding the need to use multiple high-spatial-resolution reference sources to increase the robustness of validations. Furthermore, it highlights the importance of caution when applying global products in regional validations without proper local adaptation. This result also corroborates the findings of Alencar et al. [27]; Silva Junior et al. [58], Hoffmann et al. [36], and Arruda et al. [67], who identified MapBiomas as a robust reference dataset for the Brazilian territory due to its local calibration and regional adaptation.

This behavior may be related to methodological differences between the two reference datasets, including detection algorithms, temporal composition strategies, and false-positive minimization criteria [36,52]. While MapBiomas Fire uses a Deep Neural Network (DNN) approach regionally calibrated for Brazilian biomes, GABAM employs a Random Forest-based pipeline with global calibration [67]. As discussed by Long et al. [46] and Zhang et al. [48], global reference systems may exhibit greater variability in fragmented tropical landscapes, which may partly explain the higher false positives obtained when the evaluated products were compared against GABAM. Pessôa et al. [68] highlight that GABAM has a good capacity to detect small burned areas; however, it also presents limitations due to the limited revisit frequency of the Landsat series satellites and reduced detection of burned areas in cloudy and rainy tropical regions such as the Amazon, where burned areas may be underestimated. On the other hand, it is important to emphasize that GABAM is among the few globally available 30 m burned area datasets; furthermore, it has been used as a reference product in the studies by Zhang et al. [48] and Guo et al. [50] and has shown high performance in comparison with other products, as observed in Qi et al. [69], Ferro et al. [10], Gonzalez-Ibarzabal et al. [70], and Wang et al. [71]. Therefore, future assessments in the Amazon should prioritize regional reference datasets or combine multiple sources to reduce methodological biases.

The two reference datasets differed substantially in the total burned area mapped within the Xingu River basin in 2024. MapBiomas Fire mapped approximately 40,800 km^2, whereas GABAM mapped 12,500 km^2, representing a difference of approximately 28,300 km^2 and a 69% lower burned area extent in GABAM. This substantial difference in mapped extent directly affects the confusion matrix components: the smaller burned area extent represented by GABAM increases the potential area classified as FP for the evaluated products while constraining the potential FN area. Therefore, the contrasting CE and OE values obtained against the two references should be interpreted partly as a consequence of differences in reference burned area extent rather than solely as differences in product performance. Beyond the comparative evaluation of individual burned area products, the results of this study demonstrate that validation outcomes in complex tropical forests are strongly conditioned by the reference dataset used, the spatial scale of analysis, and the landscape context. The contrasting results obtained with MapBiomas Fire and GABAM show that product performance cannot be interpreted independently of the validation framework, particularly in Amazonian environments where burned scars are frequently fragmented, spectrally complex, and strongly influenced by land cover conditions. Therefore, the combined use of regional and global reference datasets provides a more complete understanding of product behavior and helps identify the methodological conditions under which each product performs more reliably.

5.4. Implications for Forest Fire Monitoring and Management

Reliable burned area information is essential for wildfire surveillance, post-fire assessment, conservation planning, and the prioritization of prevention and response activities. High OE may underrepresent small, fragmented, or forest understory fires, whereas high CE may exaggerate burned extent or reduce the spatial precision of impact assessment. These limitations are particularly relevant in heterogeneous tropical forest landscapes, where monitoring resources and field verification may be spatially constrained.

The results support a multi-source approach to operational monitoring. FireCCIS311 may be preferable when spatial agreement and the representation of medium-to-large burned scars are priorities, whereas AQ1Km may provide complementary sensitivity when minimizing omission is particularly important, provided that its higher CE is considered. The marked differences obtained using MapBiomas Fire and GABAM also show that

machine-learning-based reference datasets should not be assumed to be interchangeable when benchmarking burned area products. Regional and global references should therefore be interpreted together whenever possible to obtain a more robust assessment of product performance.

5.5. Limitations of the Study and Future Perspectives

The 30 m reference data used in this study (MapBiomas and GABAM) are not without uncertainties. Both are derived from Landsat images, whose temporal resolution varies between 8 and 16 days depending on the combination of Landsat sensors, and whose spatial coverage is conditioned by the path/row acquisition system. These limitations can result in signal loss associated with the time lag between acquisitions, as well as underestimation of small and short-duration fires, introducing inherent uncertainties when compared with global products based on more frequent observations [68,72]. Furthermore, although the analyzed year was characterized by extreme forest fire activity, this analysis focused on a single year and did not consider the interannual variability of fire patterns in the region. Therefore, future studies should broaden the temporal approach by incorporating monthly analyses and multi-year series in order to assess the stability and consistency of the products under different climatic conditions and fire regimes. It is also recommended to include independent validations based on field data or higher-spatial-resolution imagery, such as PlanetScope and Sentinel-2, allowing for a refined assessment of the spatial accuracy of burned scars [73]. It is important to emphasize that active fire hotspot data have their own spatial and temporal uncertainties; therefore, this factor should be considered when interpreting hit probability density maps. Because active fire observations are also incorporated into the generation of some evaluated burned area products, the hotspot density analysis should be regarded as a complementary consistency assessment rather than a fully independent validation.

An important limitation concerns the trade-off between spatial detail and temporal and operational availability. Although both reference datasets provide burned area information at 30 m resolution, MapBiomas Fire offers annual and monthly mapping, whereas GABAM is an annual post-processed product. In contrast, the four evaluated products provide monthly information. Thus, the finer spatial resolution of reference datasets does not necessarily imply greater operational suitability. While high-resolution datasets provide more detailed representations of burned scar boundaries and small patches, annual products such as GABAM are more appropriate for retrospective assessment and validation than for timely or intra-annual monitoring. Conversely, monthly moderate- and coarse-resolution products provide less spatial detail but may better support operational monitoring. Therefore, dataset selection should consider not only mapping accuracy and spatial resolution but also temporal frequency, data availability, and the specific requirements of the intended application. An additional limitation is the temporal scope of the analysis, which was restricted to 2024, a severe fire season in the Xingu River basin. Therefore, the performance patterns observed here may not be directly transferable to years characterized by different fire regimes, burned area extent, patch size distributions, or environmental and atmospheric conditions. Future studies should extend this assessment to multiple years encompassing contrasting fire seasons to evaluate the temporal stability of product performance and determine whether the patterns identified in 2024 persist under different fire conditions.

Although the Xingu basin represents a key area of the Amazonian Deforestation Arc, its hydroclimatic and structural particularities may limit the extrapolation of results to other regions. Thus, future studies should consider areas with different environmental characteristics, including transition zones between biomes and drier regions of Brazil, such as the central and northeastern regions, where fire regimes, vegetation structure, and

landscape dynamics exhibit distinct behaviors [3,63,74]. Finally, for future operational monitoring in the Amazon, it is recommended to combine complementary products, for example, FireCCIS311 for detecting medium- to large-sized burned scars and AQ1Km to maximize sensitivity in agricultural frontier areas, in addition to the use of regional references such as MapBiomas Fire. The development of hybrid products that integrate active fire data and higher-resolution reflectance (30–100 m) on cloud computing platforms, such as Google Earth Engine, represents a promising direction to reduce the current OE in small fires and CE in heterogeneous landscapes. Overall, these findings highlight that burned area product selection in the Amazon should be guided not only by global accuracy metrics but also by the intended application, the dominant fire regime, the spatial scale of analysis, the reference dataset used for validation, and the characteristics of the landscape. Future validation efforts should therefore prioritize multi-source approaches that combine regional reference datasets, active fire information, and higher-spatial-resolution imagery to reduce OE in small fires and CE in heterogeneous landscapes. This is particularly relevant under changing climatic conditions, where increasing drought stress and land use pressure may alter fire behavior and increase the need for reliable, regionally validated monitoring systems to support forest risk assessment, wildfire management, and decision-making in tropical regions.

6. Conclusions

This study provides a comparative assessment of the AQ1Km, FireCCIS311, MCD64A1, and VNP64A1 burned area products in the Xingu River basin during the severe 2024 fire season, using MapBiomas Fire and GABAM as separate higher-spatial-resolution reference datasets. Based on the complementary accuracy, geometric, patch size, land use and land cover, spatial regression, and active fire hotspot analyses, the main findings and corresponding conclusions can be summarized as follows:

(1) FireCCIS311 showed the most consistent overall performance among the evaluated products. It achieved the highest spatial agreement with MapBiomas Fire (IoU = 52.67%), better geometric coherence of burned scars, and the strongest relationship in the 5 × 5 km grid regression analysis (r^2 = 0.88; RMSE = 5.31 percentage points). These results indicate that FireCCIS311 provides a comparatively balanced representation of burned area extent and spatial patterns, particularly for medium-to-large and more continuous burned scars in the Xingu basin.

(2) The evaluated products exhibited distinct trade-offs between sensitivity, omission, and spatial precision. AQ1Km showed greater sensitivity and stronger spatial association with active fire hotspots, but this behavior was accompanied by higher commission errors and spatial overestimation. In contrast, MCD64A1 and VNP64A1 showed more selective detection and intermediate overall performance, but with omission errors of approximately 50% in the pixel-based assessment. Therefore, no single product performs equally well for all aspects of burned area detection, and product selection should consider the intended application and the relative importance of omission versus commission errors.

(3) Burned scar size, geometry, and land cover context strongly affected product performance. All products showed greater difficulty in detecting small and fragmented burned patches, whereas agreement generally improved for larger and more continuous scars. Detection was also more consistent in savanna formations and pasture than in forest formations and flooded forests, where closed canopy, shading, landscape fragmentation, and understory burning can reduce the spectral detectability of fire effects. Consequently, burned area products should be interpreted cautiously in heterogeneous and densely forested Amazonian landscapes, particularly when small or fragmented fires are of interest.

(4) Validation outcomes were strongly dependent on the reference dataset used. All evaluated products showed substantially greater agreement with MapBiomas Fire than with GABAM, while the two reference datasets themselves differed in the extent, continuity, and fragmentation of mapped burned scars. These differences demonstrate that higher-spatial-resolution automated reference datasets should not be treated as interchangeable or error-free ground truth. The choice of reference framework is therefore a relevant source of uncertainty in burned area product validation and should be explicitly considered when interpreting accuracy metrics.

(5) A complementary, multi-source approach provides the most robust basis for operational burned area monitoring in heterogeneous tropical landscapes. FireCCIS311 is particularly suitable when spatial agreement and representation of medium-to-large burned scars are priorities, whereas AQ1Km can provide complementary sensitivity in areas with intense fire activity, provided that its higher commission error is considered. Combining burned area products with regionally appropriate reference information and complementary active fire observations can therefore reduce dependence on the limitations of any single dataset and improve the interpretation of burned area patterns for wildfire monitoring, post-fire assessment, and fire management in the Brazilian Amazon.

Overall, the results demonstrate that burned area product performance in the Xingu River basin depends not only on sensor characteristics and algorithm design, but also on burned scar size, landscape context, spatial resolution, and the reference dataset adopted for validation. Because the present assessment focused on the severe 2024 fire season, future studies should evaluate the temporal stability of these findings using multi-year analyses, contrasting fire seasons, and independent higher-spatial-resolution or field-based reference data.

Author Contributions: Conceptualization, J.A.d.S.J.; Formal analysis, J.A.d.S.J., A.d.P.P. and A.M.R.-A.; Investigation, J.A.d.S.J., A.d.P.P., A.M.R.-A., J.A.E.S.d.S. and L.M.M.d.O.; Methodology, J.A.d.S.J., A.d.P.P., A.M.R.-A., J.A.E.S.d.S. and L.M.M.d.O.; Writing—original draft, J.A.d.S.J., A.d.P.P., A.M.R.-A. and L.M.M.d.O.; Writing—review and editing, J.A.d.S.J., A.d.P.P., A.M.R.-A. and L.M.M.d.O. All authors have read and agreed to the published version of the manuscript.

Funding: The article processing charge (APC) was funded by the University of Jaén, Spain. The first author received a scholarship from the Coordination for the Improvement of Higher Education Personnel (CAPES, Brazil). This research also benefited from institutional support provided by the Department of Cartographic Engineering and Surveying (DECart) and the Graduate Program in Civil Engineering (Water Resources) (PPGEC) at the Federal University of Pernambuco (UFPE, Brazil), the Center for Advanced Studies on Earth Sciences, Energy and Environment (CEACTEMA) at the University of Jaén (Spain), and the RNM-282 Research Group of the Junta de Andalucía (Spain).

Data Availability Statement: The data used in this study were derived from resources available in the public domain. The source datasets are available from the following repositories: AQ1Km Burned Area Product (https://data.inpe.br/queimadas/portal/dados-abertos/#da-area-qmd, accessed on 2 April 2026); ESA Fire_cci Sentinel-3 SYN Burned Area Pixel Product version 1.1—FireCCIS311 (https://climate.esa.int/en/catalogue/d441079fc77f49fabeb41330612b252f/, accessed on 2 April 2026); MODIS MCD64A1 Collection 6.1 (https://doi.org/10.5067/MODIS/MCD64A1.061, accessed on 2 April 2026); VIIRS VNP64A1 version 1 (https://doi.org/10.5067/VIIRS/VNP64A1.001, accessed on 2 April 2026); MapBiomas Fire Collection 4 (https://brasil.mapbiomas.org/, accessed on 2 April 2026); the updated 30 m Global Annual Burned Area Map—GABAM, 2014–2024 (https://doi.org/10.5281/zenodo.13858799, accessed on 2 April 2026); the BDQueimadas active fire hotspot database (https://terrabrasilis.dpi.inpe.br/queimadas/bdqueimadas/, accessed on 2 April 2026); and the Metadata Catalog of the Brazilian National Water and Basic Sanitation Agency—ANA (https://metadados.snirh.gov.br, accessed on 2 April 2026). The processed data supporting the figures, tables, and statistical analyses are available from the corresponding author upon reasonable request.

Acknowledgments: The authors acknowledge the CNPq/Brazil Research Group "Remote Sensing and Machine Learning Applied to Geoenvironmental Studies", coordinated by Admilson P. Pacheco, for its scientific and institutional support. During the preparation of this manuscript, the authors used ChatGPT (OpenAI, GPT-6 Model Astra) to assist in the preparation of the methodological workflow figure and graphical abstract. The authors reviewed and edited the AI-assisted content and take full responsibility for the published material.

Conflicts of Interest: The authors declare no conflicts of interest.

References

1. Araújo, A.N.M.; Chiodi Pereira, E.; de Almeida Piai, K.; da Costa Dias, T.; Polido Kaneshiro Olympio, K. Entre a fumaça de incêndios florestais, cinzas e rios: Relato de campo para biomonitoramento de brigadistas florestais na Amazônia. *Rev. Pan-Amaz. Saúde* **2025**, *16*, e202501792. [CrossRef]
2. Alencar, A.; Arruda, V.; Martenexen, F.; Reis Rosa, E. Fogo no Brasil em 2024: O Retrato Fundiário da Área Queimada nos Biomas. Available online: https://acervo.socioambiental.org/sites/default/files/documents/m1d00064.pdf (accessed on 30 June 2026).
3. Silva, R.M.d.; Lopes, A.G.; Santos, C.A.G. Deforestation and fires in the Brazilian Amazon from 2001 to 2020: Impacts on rainfall variability and land surface temperature. *J. Environ. Manag.* **2023**, *326*, 116664. [CrossRef] [PubMed]
4. da Veiga, R.M.; Barbosa, M.L.F.; Spuler, F.R.; Ferreira, I.J.M.; Mindlin, J.; Kelley, D.I.; Matusevich, V.; Rodrigues, R.R.; Alencar, A.; Ratilla, D.C.; et al. Recognition of loss & damage from wildfires is key for climate justice. *Commun. Earth Environ.* **2025**, *6*, 898. [CrossRef] [PubMed]
5. Oliveira, A.C.; Sehn Körting, T. A multi-temporal dataset for mapping burned areas in the Brazilian Cerrado using time series of remote sensing imagery. *Big Earth Data* **2025**, *9*, 473–504. [CrossRef]
6. Liu, P.; Liu, Y.; Guo, X.; Liu, Y.; Zhao, W.; Xu, W. Faster, better, and more accurate mapping of burned areas using Sentinel-2 multispectral images. *Remote Sens. Environ.* **2026**, *333*, 115137. [CrossRef]
7. Chuvieco, E.; Mouillot, F.; van der Werf, G.R.; San Miguel, J.; Tanase, M.; Koutsias, N.; García, M.; Yebra, M.; Padilla, M.; Gitas, I.; et al. Historical background and current developments for mapping burned area from satellite Earth observation. *Remote Sens. Environ.* **2019**, *225*, 45–64. [CrossRef]
8. Bastarrika, A.; Rodriguez-Montellano, A.; Roteta, E.; Hantson, S.; Franquesa, M.; Torre, L.; Gonzalez-Ibarzabal, J.; Artano, K.; Martinez-Blanco, P.; Mesanza, A.; et al. An automatic procedure for mapping burned areas globally using Sentinel-2 and VIIRS/MODIS active fires in Google Earth Engine. *ISPRS J. Photogramm. Remote Sens.* **2024**, *218*, 232–245. [CrossRef]
9. Ramos, C.J.P.; Graça, P.M.L.d.A.; Fearnside, P.M. Adjusted ΔNBR index thresholds for forest fire severity mapping: A study in Central Amazonia. *Land Degrad. Dev.* **2025**, *36*, 1844–1859. [CrossRef]
10. Ferro, P.D.; Mataveli, G.; Arcanjo, J.d.S.; Dutra, D.J.; de Medeiros, T.P.; Shimabukuro, Y.E.; Pessôa, A.C.M.; de Oliveira, G.; Anderson, L.O. Regional-scale assessment of burn scar mapping in Southwestern Amazonia using burned area products and CBERS/WFI data cubes. *Fire* **2024**, *7*, 67. [CrossRef]
11. Giglio, L.; Boschetti, L.; Roy, D.P.; Humber, M.L.; Justice, C.O. The Collection 6 MODIS burned area mapping algorithm and product. *Remote Sens. Environ.* **2018**, *217*, 72–85. [CrossRef] [PubMed]
12. Boschetti, L.; Roy, D.P.; Giglio, L.; Huang, H.; Zubkova, M.; Humber, M.L. Global validation of the Collection 6 MODIS burned area product. *Remote Sens. Environ.* **2019**, *235*, 111490. [CrossRef] [PubMed]
13. Giglio, L.; Boschetti, L.; Roy, D.P.; Hall, J.V.; Zubkova, M.; Humber, M.; Huang, H.; Oles, V. The NASA VIIRS burned area product, global validation, and intercomparison with the NASA MODIS burned area product. *Remote Sens. Environ.* **2025**, *331*, 115006. [CrossRef]
14. Chuvieco, E.; Lizundia-Loiola, J.; Pettinari, M.L.; Ramo, R.; Padilla, M.; Tansey, K.; Mouillot, F.; Laurent, P.; Storm, T.; Heil, A.; et al. Generation and analysis of a new global burned area product based on MODIS 250 m reflectance bands and thermal anomalies. *Earth Syst. Sci. Data* **2018**, *10*, 2015–2031. [CrossRef]
15. Lizundia-Loiola, J.; Otón, G.; Ramo, R.; Chuvieco, E. A spatio-temporal active-fire clustering approach for global burned area mapping at 250 m from MODIS data. *Remote Sens. Environ.* **2020**, *236*, 111493. [CrossRef]
16. Lizundia-Loiola, J.; Franquesa, M.; Boettcher, M.; Kirches, G.; Pettinari, M.L.; Chuvieco, E. Implementation of the burned area component of the Copernicus Climate Change Service: From MODIS to OLCI data. *Remote Sens.* **2021**, *13*, 4295. [CrossRef]
17. Padilla, M.; Ramo, R.; Gomez-Dans, J.L.; Sierra, S.; Mota, B.; Lacaze, R.; Tansey, K. Near-real time monitoring of burned area at global scale based on deep learning. *Int. J. Remote Sens.* **2025**, *46*, 5996–6038. [CrossRef]
18. Lizundia-Loiola, J.; Franquesa, M.; Khairoun, A.; Chuvieco, E. Global burned area mapping from Sentinel-3 Synergy and VIIRS active fires. *Remote Sens. Environ.* **2022**, *282*, 113298. [CrossRef]
19. Alonso-Canas, I.; Chuvieco, E. Global burned area mapping from ENVISAT-MERIS and MODIS active fire data. *Remote Sens. Environ.* **2015**, *163*, 140–152. [CrossRef]

20. Libonati, R.; DaCamara, C.; Setzer, A.; Morelli, F.; Melchiori, A. An algorithm for burned area detection in the Brazilian Cerrado using 4 μm MODIS imagery. *Remote Sens.* **2015**, *7*, 15782–15803. [CrossRef]
21. Silva, P.S.; Rodrigues, J.A.; Nogueira, J.; Moura, L.C.; Enout, A.; Cuiabália, C.; DaCamara, C.C.; Pereira, A.A.; Libonati, R. Joining forces to fight wildfires: Science and management in a protected area of Pantanal, Brazil. *Environ. Sci. Policy* **2024**, *159*, 103818. [CrossRef]
22. Fornacca, D.; Ren, G.; Xiao, W. Performance of three MODIS fire products (MCD45A1, MCD64A1, MCD14ML), and ESA Fire_CCI in a mountainous area of Northwest Yunnan, China, characterized by frequent small fires. *Remote Sens.* **2017**, *9*, 1131. [CrossRef]
23. Matveev, A.M.; Bartalev, S.A.; Egorov, V.A.; Saigin, I.A.; Stytsenko, F.V.; Shinkarenko, S.S. Validation of national and global satellite-derived products for mapping burned areas in Russia. *Cosm. Res.* **2025**, *63*, S151–S164. [CrossRef]
24. Stroppiana, D.; Sali, M.; Brivio, P.A.; Sona, G.; Franquesa, M.; Pettinari, M.L.; Chuvieco, E. Spatial agreement of burned area products derived from very high- to coarse-resolution satellite imagery in African biomes. *Fire* **2025**, *8*, 126. [CrossRef]
25. Román, M.O.; Justice, C.; Paynter, I.; Boucher, P.B.; Devadiga, S.; Endsley, A.; Erb, A.; Friedl, M.; Gao, H.; Giglio, L.; et al. Continuity between NASA MODIS Collection 6.1 and VIIRS Collection 2 land products. *Remote Sens. Environ.* **2024**, *302*, 113963. [CrossRef]
26. Pacheco, A.d.P.; Silva Junior, J.A.d.; Ruiz-Armenteros, A.M.; Henriques, R.F.F. Assessment of k-nearest neighbor and random forest classifiers for mapping forest fire areas in Central Portugal using Landsat-8, Sentinel-2, and Terra imagery. *Remote Sens.* **2021**, *13*, 1345. [CrossRef]
27. Alencar, A.A.C.; Arruda, V.L.S.; da Silva, W.V.; Conciani, D.E.; Costa, D.P.; Crusco, N.; Duverger, S.G.; Ferreira, N.C.; Franca-Rocha, W.; Hasenack, H.; et al. Long-term Landsat-based monthly burned area dataset for the Brazilian biomes using deep learning. *Remote Sens.* **2022**, *14*, 2510. [CrossRef]
28. Valencia, G.M.; Anaya, J.A.; Velásquez, É.A.; Ramo, R.; Caro-Lopera, F.J. About validation-comparison of burned area products. *Remote Sens.* **2020**, *12*, 3972. [CrossRef]
29. Parente, J.; Girona-García, A.; Lopes, A.R.; Keizer, J.J.; Vieira, D.C.S. Prediction, validation, and uncertainties of a nation-wide post-fire soil erosion risk assessment in Portugal. *Sci. Rep.* **2022**, *12*, 2945. [CrossRef] [PubMed]
30. Ribeiro, A.F.S.; Santos, L.; Randerson, J.T.; Uribe, M.R.; Alencar, A.A.C.; Macedo, M.N.; Morton, D.C.; Zscheischler, J.; Silvestrini, R.A.; Rattis, L.; et al. The time since land-use transition drives changes in fire activity in the Amazon-Cerrado region. *Commun. Earth Environ.* **2024**, *5*, 96. [CrossRef]
31. Hall, J.V.; Argueta, F.; Giglio, L. Validation of MCD64A1 and FireCCI51 cropland burned area mapping in Ukraine. *Int. J. Appl. Earth Obs. Geoinf.* **2021**, *102*, 102443. [CrossRef]
32. Padilla, M.; Wheeler, J.; Tansey, K. ESA CCI ECV Fire Disturbance: D4.1.1 Product Validation Report, Version 2.1. Available online: https://climate.esa.int/media/documents/Fire_cci_D4.1.1_PVR_v2.1.pdf (accessed on 30 June 2026).
33. Huang, Y.; Pan, Y.; Xia, X.; Zhou, Q.; Chen, Q.; Zhang, S. Validating MCD64A1 and FireCCI51 burned area mapping in the Qinghai-Tibetan Plateau. *Geocarto Int.* **2023**, *38*, 2285345. [CrossRef]
34. Khairoun, A.; Ciais, P.; Nguyen, T.H.; Qiu, C.; Fang, C.; Aires, F.; Veraverbeke, S.; Delcourt, C.J.F.; Zheng, B.; Chuvieco, E. Peat fires contribute disproportionately to Siberian fire carbon emissions. *Sci. Adv.* **2026**, *12*, eadl2368. [CrossRef] [PubMed]
35. Chandel, A.; Sarwat, W.; Najah, A.; Dhanagare, S.; Agarwala, M. Evaluating methods to map burned area at 30-meter resolution in forests and agricultural areas of Central India. *Front. For. Glob. Chang.* **2022**, *5*, 933807. [CrossRef]
36. Hoffmann, T.B.; Arai, E.; Shimabukuro, Y.E.; Adami, M. Mapping burned areas in Cerrado protected areas (2000–2020): A comparative analysis of Landsat classification, MapBiomas Fire, and MCD64A1. In *Proceedings of the 2025 Latin American GRSS & ISPRS Remote Sensing Conference (LAGIRS)*; IEEE: Piscataway, NJ, USA, 2025; pp. 1–7. [CrossRef]
37. Eufemia, L.; Dias Turetta, A.P.; Bonatti, M.; Da Ponte, E.; Sieber, S. Fires in the Amazon region: Quick policy review. *Dev. Policy Rev.* **2022**, *40*, e12620. [CrossRef]
38. Metadata Catalog of the National Water and Basic Sanitation Agency (ANA). Available online: https://metadados.snirh.gov.br (accessed on 30 June 2026).
39. Henrique, A.; Maffioletti, F.D.; Biazatti, L.D.; Carvalho, G.S.; Pinheiro da Silva, M.A.; Trajano, K.; Pereira, J.; Teixeira, E.; Santos, M.M. Temporal evolution of deforestation in the Xingu River Watershed between 2008 and 2020. *Adv. For. Sci.* **2024**, *11*, 2168–2175. [CrossRef]
40. Lucas-Borja, M.E. Wildfires and Desertification: The Role of Fire Regime. In *The Labyrinth of Desertification*; Springer: Cham, Switzerland, 2026; pp. 59–66. [CrossRef]
41. Giglio, L. *VIIRS/NPP Burned Area Monthly L4 Global 500 m SIN Grid V001*; NASA Land Processes Distributed Active Archive Center: Sioux Falls, SD, USA, 2019. [CrossRef]
42. Bento-Gonçalves, A.; Vieira, A.; dos Santos, S.M. Research on Wildfires, Soil Erosion and Land Degradation in the XXI Century. *Fire* **2024**, *7*, 327. [CrossRef]
43. Mapbiomas Fire Monitor Do Fogo–MapBiomas Brasil. Available online: https://brasil.mapbiomas.org/iniciativas-e-produtos/fogo/monitor-do-fogo/ (accessed on 26 September 2026).

44. Roy, S. 30m Global Annual Burned Area Maps (GABAM)–Awesome-Gee-Community-Catalog. Available online: https://gee-community-catalog.org/projects/gabam/ (accessed on 26 September 2026).
45. Boschetti, L.; Roy, D.; Justice, C. International Global Burned Area Satellite Product Validation Protocol, Part I: Production and Standardization of Validation Reference Data. Available online: https://lpvs.gsfc.nasa.gov/PDF/BurnedAreaValidationProtocol.pdf (accessed on 30 June 2026).
46. Long, T.; Zhang, Z.; He, G.; Jiao, W.; Tang, C.; Wu, B.; Zhang, X.; Wang, G.; Yin, R. 30 m resolution global annual burned area mapping based on Landsat images and Google Earth Engine. *Remote Sens.* **2019**, *11*, 489. [CrossRef]
47. USGS Fire, Ecosystems, Climate: It's Complicated | U.S. Geological Survey. Available online: https://www.usgs.gov/news/featured-story/fire-ecosystems-climate-its-complicated (accessed on 26 September 2026).
48. Zhang, Z.; Qi, B.; Long, T.; He, G.; Wei, M. *Updated 30 m Resolution Global Annual Burned Area Map, 2014–2024*; Zenodo: Geneva, Switzerland, 2024. [CrossRef]
49. Zhang, Z.; Qi, B.; He, G.; Wang, M.; Huang, S.; Long, T.; Wang, G.; Xu, Z. High-resolution global forest burned area change monitoring using Landsat 7/8 images. *Geo-Spat. Inf. Sci.* **2025**, *28*, 2808–2821. [CrossRef]
50. Guo, Z.; Li, W.; Ciais, P.; Sitch, S.; van der Werf, G.R.; Bowring, S.P.K.; Bastos, A.; Mouillot, F.; He, J.; Sun, M.; et al. Reconstructed global monthly burned area maps from 1901 to 2020. *Earth Syst. Sci. Data* **2025**, *17*, 3599–3618. [CrossRef]
51. Uhl, J.H.; Leyk, S. Assessing the relationship between morphology and mapping accuracy of built-up areas derived from global human settlement data. *GIScience Remote Sens.* **2022**, *59*, 1722–1748. [CrossRef] [PubMed]
52. Jiao, L.; Liu, Y.; Li, H. Characterizing land-use classes in remote sensing imagery by shape metrics. *ISPRS J. Photogramm. Remote Sens.* **2012**, *72*, 46–55. [CrossRef]
53. BDQueimadas Program. Available online: https://terrabrasilis.dpi.inpe.br/queimadas/bdqueimadas/ (accessed on 30 June 2026).
54. Franquesa, M.; Stehman, S.V.; Chuvieco, E. Assessment and characterization of sources of error impacting the accuracy of global burned area products. *Remote Sens. Environ.* **2022**, *280*, 113214. [CrossRef]
55. Shimabukuro, Y.E.; Dutra, A.C.; Arai, E.; Duarte, V.; Cassol, H.L.G.; Pereira, G.; Cardozo, F.d.S. Mapping burned areas of Mato Grosso State, Brazilian Amazon, using multisensor datasets. *Remote Sens.* **2020**, *12*, 3827. [CrossRef]
56. Katagis, T.; Gitas, I.Z. Assessing the accuracy of MODIS MCD64A1 C6 and FireCCI51 burned area products in Mediterranean ecosystems. *Remote Sens.* **2022**, *14*, 602. [CrossRef]
57. Ouattara, B.; Thiel, M.; Sponholz, B.; Paeth, H.; Yebra, M.; Mouillot, F.; Kacic, P.; Hackman, K. Enhancing burned area monitoring with VIIRS dataset: A case study in Sub-Saharan Africa. *Sci. Remote Sens.* **2024**, *10*, 100165. [CrossRef]
58. Silva Junior, J.A.d.; Pacheco, A.d.P.; Ruiz-Armenteros, A.M.; Henriques, R.F.F. Comparative analysis between remote sensing burned area products in Brazil: A case study in an environmentally unstable watershed. *Fire* **2024**, *7*, 238. [CrossRef]
59. Pereira, A.A.; Pereira, J.M.C.; Libonati, R.; Setzer, A.W.; Oom, D.; Morelli, F.; Carvalho, L.M.T.; Machado-Silva, F. Burned area mapping in the Brazilian Savanna using a one-class support vector machine trained by active fires. *Remote Sens.* **2017**, *9*, 1161. [CrossRef]
60. Padilla, M.; Ramo, R.; Gomez-Dans, J.L.; Sierra, S.; Mota, B.; Lacaze, R.; Tansey, K. Global near-real-time burned area mapping using Sentinel-2 and VIIRS active fires. *Fire* **2026**, *9*, 195. [CrossRef]
61. Fornacca, D.; Ye, Y.; Li, X.; Xiao, W. Including small fires in global historical burned area products: Promising results from a Landsat-based product. *Fire* **2025**, *8*, 422. [CrossRef]
62. Shimabukuro, Y.E.; de Oliveira, G.; Pereira, G.; Arai, E.; Cardozo, F.; Dutra, A.C.; Mataveli, G. Assessment of burned areas during the Pantanal fire crisis in 2020 using Sentinel-2 images. *Fire* **2023**, *6*, 277. [CrossRef]
63. Boschetti, L.; Stehman, S.V.; Roy, D.P. A stratified random sampling design in space and time for regional to global scale burned area product validation. *Remote Sens. Environ.* **2016**, *186*, 465–478. [CrossRef] [PubMed]
64. Santana, N.; de Carvalho Júnior, O.; Gomes, R.; Guimarães, R. Burned-area detection in Amazonian environments using standardized time series per pixel in MODIS data. *Remote Sens.* **2018**, *10*, 1904. [CrossRef]
65. Correa, D.B.; Alcântara, E.; Libonati, R.; Massi, K.G.; Park, E. Increased burned area in the Pantanal over the past two decades. *Sci. Total Environ.* **2022**, *835*, 155386. [CrossRef] [PubMed]
66. Santos, F.C.; Chaves, F.M.; Negri, R.G.; Massi, K.G. Fires in Pantanal: The link to agriculture, conversions in Cerrado, and hydrological changes. *Wetlands* **2024**, *44*, 75. [CrossRef]
67. Arruda, V.L.d.S.; Alencar, A.A.C.; de Carvalho Júnior, O.A.; de Figueiredo Ribeiro, F.; de Arruda, F.V.; Conciani, D.E.; da Silva, W.V.; Shimbo, J.Z. Assessing four decades of fire behavior dynamics in the Cerrado biome (1985 to 2022). *Fire Ecol.* **2024**, *20*, 64. [CrossRef]
68. Pessôa, A.C.M.; Anderson, L.O.; Carvalho, N.S.; Campanharo, W.A.; Silva Junior, C.H.L.; Rosan, T.M.; Reis, J.B.C.; Pereira, F.R.S.; Assis, M.; Jacon, A.D.; et al. Intercomparison of burned area products and its implication for carbon emission estimations in the Amazon. *Remote Sens.* **2020**, *12*, 3864. [CrossRef]

69. Qi, B.; Zhang, Z.; Long, T.; He, G.; Wang, G.; Peng, Y.; Xu, Z. High-resolution (30 m) burned area product improves the ability for carbon emission estimation in Africa. *Earth's Future* **2024**, *12*, e2024EF005051. [CrossRef]
70. Gonzalez-Ibarzabal, J.; Bastarrika, A.; Stehman, S.V.; Stroppiana, D.; Franquesa, M. S2BAVG: A global Sentinel-2 grid for burned area product validation. *Int. J. Appl. Earth Obs. Geoinf.* **2025**, *144*, 104889. [CrossRef]
71. Wang, Y.; Zhang, Z.; Ni, W.; Guo, Z. Burned area mapping of boreal forests using automatically generated samples. In *Proceedings of IGARSS 2025—2025 IEEE International Geoscience and Remote Sensing Symposium*; IEEE: Piscataway, NJ, USA, 2025; pp. 3500–3504. [CrossRef]
72. Dutra, D.J.; Fearnside, P.M.; Yanai, A.M.; Dalagnol, R.; Cabral, A.C.; Burton, C.; Jones, C.; Betts, R.; Ferro, P.D.; Braga, D.A.; et al. Burned area mapping in different data products for the southwest of the Brazilian Amazon. *Rev. Bras. Cartogr.* **2023**, *75*, 1–16. [CrossRef]
73. Gaveau, D.L.A.; Descals, A.; Salim, M.A. Nationwide monthly burned area monitoring in Indonesia using Sentinel-2. *PLoS ONE* **2026**, *21*, e0331831. [CrossRef] [PubMed]
74. Silva Junior, J.A.d.; Pacheco, A.d.P.; Ruiz-Armenteros, A.M.; Henriques, R.F.F. Evaluation of the ability of SLSTR (Sentinel-3B) and MODIS (Terra) images to detect burned areas using spatial-temporal attributes and SVM classification. *Forests* **2023**, *14*, 32. [CrossRef]

Disclaimer/Publisher's Note: The statements, opinions and data contained in all publications are solely those of the individual author(s) and contributor(s) and not of MDPI and/or the editor(s). MDPI and/or the editor(s) disclaim responsibility for any injury to people or property resulting from any ideas, methods, instructions or products referred to in the content.